Nuclear Structure Corrections in Muonic Deuterium

by

Oscar Javier Hernandez

A thesis submitted to
The Faculty of Graduate Studies of
The University of Manitoba
in partial fulfillment of the requirements
of the degree of

Master of Science

Department of Physics and Astronomy
The University of Manitoba
Winnipeg, Manitoba, Canada
June 2015

Nuclear Structure Corrections in Muonic Deuterium

Abstract

The 7σ discrepancy between the charge radius of the proton as extracted from electronic hydrogen to the determination from muonic hydrogen, coined the proton "radius puzzle", challenges our understanding of physics based on the standard model. High-precision measurements have been conducted on muonic deuterium to study whether the discrepancy with ordinary atoms persists or varies with mass number. For the success of this experimental campaign accurate theoretical calculations of the nuclear structure corrections in muonic deuterium (μD) are required. In this work we contributed by accurately and precisely calculating them using state-of-the-art nuclear potentials derived from chiral effective field theory. We performed a multipole expansion of the electromagnetic operator and accounted for Coulomb, relativistic and finite-nucleon-size corrections. Our determinations will impact the accuracy of the experimental program.

Contents

List of Figures

List of Tables

Acknowledgments

I would like to begin by thanking my advisor Dr. Sonia Bacca for sharing her guidance and support through my project. I am grateful for all of the countless hours that she spent proofreading my thesis, as well as listening to and providing feedback to all of my research talks. I would also like to thank my collaborator Dr. Chen Ji who has been a very dedicated, excellent mentor to me throughout this project. I appreciate all of the time he spent reading over my work. I am also grateful to my committee for their time and patience in evaluating my thesis.

I would like to thank my brother and my sister for their support and encouragement while I pursued my studies. I am particularly grateful to my mum for her unconditional love and support during my studies. This thesis is dedicated to her and to the memory of my father. I am also grateful to my family in Guatemala for all of their support.

I would like to thank my partner for all their love and support and for tolerating my physics discussions. Finally, I also would like to thank all of my friends and others who have supported me along the way.

Chapter 1

Introduction

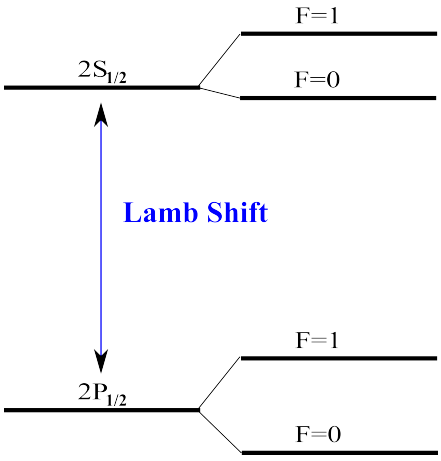

Figure 1.1: The Lamb shift splitting in hydrogen. The figure is not to scale.

First discovered by Willis Lamb, for which he was subsequently awarded the Nobel prize in physics in 1955, the Lamb shift is the $2S$-$2P$ energy difference in the spectra of the hydrogen atom illustrated in Figure 1.1. Dirac's equation for an electron interacting with a point Coulomb source predicts the concurrence of these energy levels, consequently, deviations from the point Coulomb interaction result in a non-zero energy difference. Lamb shift measurements are of interest to the nuclear physics

community because they allow the extraction of nuclear charge radii complementary to that of elastic electron scattering off nuclei.

One of the most fundamental building block of hadronic matter governing the dynamics of the observable universe is the proton. Yet many of its properties, such as its charge radius, are not well understood. The proton charge radius can be determined from elastic electron-proton scattering through an extrapolation of the electron form factor to zero momentum transfer. This extrapolation presented many difficulties for early scattering experiments due to missing radiative corrections and Coulomb distortion corrections [1, 2]. In addition, the proton charge density is strongly dependent on the low momentum region of the form factor as shown in Figure 1.2 where data is either not accurate or not available [3].

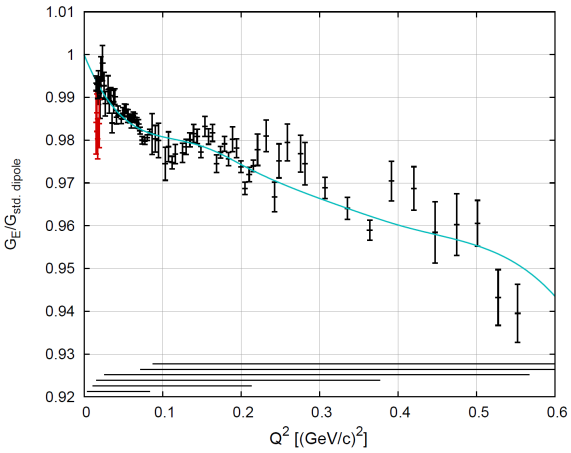

Figure 1.2: The electron hydrogen scattering cross section as a function of the momentum transfer Q^2 [4]. The horizontal black lines at the bottom of the plot indicates the Q^2 regions covered by the different energies.

The CODATA-2010 analysis has determined the proton charge radius to be $r_p = 0.8775(51)$fm [5] based on hydrogen spectroscopy and elastic electron proton scattering. However, recent measurements of the muonic hydrogen Lamb shift have determined the proton charge radius to ten-times the accuracy, $r_p = 0.84184(67)$fm [6, 7], in disagreement with previous determinations by 7σ as illustrated in Figure 1.3. This large discrepancy, amounting to a missing energy correction of 0.329 meV, has been coined the "proton radius puzzle" and challenges our understanding of physics based on the standard model. To address this puzzle, there have been new electron-proton scattering measurements conducted at the Mainz and at the Jefferson Laboratory [8, 9] and re-analysis of previous electron-scattering experiments [10, 11]. Up to date, these efforts have reinforced the puzzle.

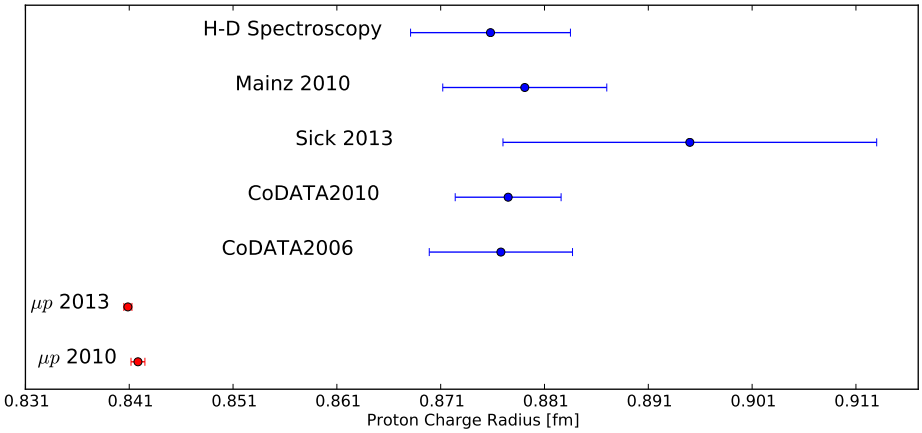

Figure 1.3: A comparison of the proton charge radius as determined from muonic hydrogen spectroscopy and electronic hydrogen determinations.

The robustness of the muonic hydrogen experiments along with the long-standing (3σ) $g-2$ anomaly [12] of the muon has led to the consideration of beyond-the-standard-model explanations such as forces that violate lepton universality to explain

both discrepancies [13, 14]. However, there has not been any widely accepted explanation of the puzzle thus far. To resolve this disagreement experimentalists have put forth proposals to conduct elastic muon-proton scattering in addition to electron-proton scattering experiments. An alternative experimental approach, proposed by the CREMA collaboration [15], is to perform additional Lamb shift measurements in muonic atoms with higher atomic masses and charge numbers, A, Z, respectively, to track any differences in the nuclear charge radii with respect to radii obtained from the spectroscopy of normal atoms or electron scattering. The Lamb shift measurement of muonic deuterium has already been completed by the collaboration and the data are being analysed. In light of this ongoing experiment, this work will focus on the nuclear structure theory of muonic deuterium.

For a muonic deuterium atom, the Lamb shift can be related to its charge radius squared $\langle r_{ch}^2 \rangle_d$ through equation (1.1). This is derived from first and second order perturbation theory (in natural units), in an expansion up to fifth order in α, where α is the fine structure constant,[1]

$$\Delta E(2S - 2P) = \delta_{QED} + \delta_{FS}(r_{ch}^2) + \delta_{TPE}. \tag{1.1}$$

Here, δ_{QED} are contributions from quantum electrodynamics, $\delta_{FS}(r_{ch}^2) = \frac{m_r^3}{12}(Z\alpha)^4 \langle r_{ch}^2 \rangle_d$ is the leading finite size correction, where m_r is the reduced mass of the muon-nucleus center of mass system. δ_{TPE} is the contribution from the two-photon exchange process that can be broken up into a sum of the elastic Zemach term δ_{Zem} and the inelastic nuclear polarization δ_{pol}, as $\delta_{TPE} = \delta_{pol} + \delta_{Zem}$. The term δ_{pol} can be further divided into the sum of two terms, $\delta_{pol} = \delta_{pol}^A + \delta_{pol}^N$, where δ_{pol}^A, δ_{pol}^N are the contributions from

[1] When higher order corrections are included other linear-in-$\langle r_{ch}^2 \rangle_d$ terms are obtained from δ_{QED}.

nuclear and nucleonic degrees of freedom, respectively. QED corrections have been calculated from theory to very high orders in $Z\alpha$ but we intend to calculate δ^A_{pol} and δ_{Zem} up to $(Z\alpha)^5$. Therefore, we do not discuss higher order terms.

Since the muon is approximately 200 times heavier than an electron, the strength of the Lamb shift is enhanced in muonic atoms relative to their electronic counterparts. The accuracy of the charge radius determination in muonic deuterium is limited by the precision of the contributing terms. The dominant QED corrections in equation (1.1), arising as a result of vacuum polarization and muon self interaction, have been calculated very precisely by several groups which are in agreement. Furthermore, the theoretical precision is better than the size of the proton radius puzzle, so it is unlikely to explain the discrepancy [16]. The bottleneck in these calculations is the uncertainty in the nuclear polarizability corrections. Ideally, to exploit experimental precision, theoretical calculations need to be accurate to 0.001 meV, nevertheless, at the current level of experimental precision the deuterium charge radius determined from the muonic deuterium experiments at PSI are expected to be more accurate than the CODATA value by a factor of three [17].

For muonic deuterium, the nuclear structure corrections have been recently calculated using forward dispersion relations and elastic scattering data [18]. However, due to the large uncertainty in the experimental data at low momentum transfers, this analysis yields a 47% error. A theoretical estimate of these corrections, with $1-2\%$ uncertainty, has been conducted using the zero-range approximation for the deuteron wave function [19], where the D-wave function of the deuteron is neglected and the S-wave function is approximated by a decaying exponential. An alternative approach

was done by Pachucki [20] using the AV18 nuclear potential. However, missing in his calculation was a precise estimate of the nuclear physics error arising from the nuclear potential along with a correct calculation of the nucleon polarizability effects and Zemach moments.

It is the goal of this project to understand the nuclear structure corrections and complement Pachucki's pioneering work with state-of-the-art nuclear potentials derived from an effective theory for describing low energy QCD to give a solid estimate of the nuclear physics uncertainty.

This thesis is organized as follows. Chapter II will be dedicated to the discussion of nucleon-nucleon forces and the deuteron. Chapter III will discuss in detail the theory of the Lamb shift splitting in light muonic atoms with careful attention paid to the derivation of the necessary nuclear structure corrections. Chapter IV will present our results including numerical benchmarks. The final chapter will give an overview of the results and provide directions for future work.

Chapter 2

The Deuteron and Nuclear Forces

The simplest nuclear bound state is the deuteron, consisting of a proton and neutron bound by the nucleon-nucleon interaction. The most pertinent experimentally determined properties of the deuteron, such as the binding energy E_0, total angular momentum J, intrinsic parity $\hat{\pi}$, total spin S, total isospin T, electric quadrupole moment Q_d, magnetic dipole moment $M1$, and the matter radius $\langle r^2_{str} \rangle^{1/2}_d$ are summarized in Table 2.1. In this chapter we will talk in more detail about these properties.

One of the goals of this thesis is to realistically describe these deuteron properties and then calculate δ_{pol} and δ_{Zem} in equation (1.1). Thus, I will first describe how we can model the deuteron.

In general, the total wave function of a nucleus can be written as a direct product of the spacial, spin and isospin components,

$$|\Psi\rangle = \left[|\phi\rangle^L_{\text{space}} \otimes |\chi^S\rangle_{\text{spin}}\right]^J \otimes |\chi^T\rangle_{\text{isospin}}. \tag{2.1}$$

The square brackets indicate the addition of orbital angular momentum L and spin S. The experimental values of the spin (S), total angular momentum (J), and parity ($\hat{\pi}$)

Quantity	Value
E_0	$-2.224573(2)^1$ MeV
$J^{\hat{\pi}}$	1^+
S	1
T	0
Q_d	$0.285783(30)^2$ fm^2
$M1$	$0.8574382284(94)^3$ μ_N
$\langle r^2_{str}\rangle^{1/2}_d$	$1.97507(78)^4$ fm

[1]Ref. [21], [2]Ref. [22], [3]Ref. [23] [4]Ref. [24]

Table 2.1: The static properties of the deuteron.

in Table 2.1 constrain the orbital angular momentum to be $L = \{0, 2\}$. Subsequently, the coordinate space wave function is,

$$\Psi(\boldsymbol{r}) = \left(\frac{u(r)}{r} \boldsymbol{Y}^M_{10}(\hat{r}) + \frac{w(r)}{r} \boldsymbol{Y}^M_{12}(\hat{r}) \right) \chi^{T=0}, \tag{2.2}$$

where $u(r)$ and $w(r)$ are the S and P -wave radial wave functions and $\boldsymbol{Y}^M_{10}(\hat{r})$, $\boldsymbol{Y}^M_{12}(\hat{r})$ are the vector spherical harmonics, defined in Appendix A. The normalization condition of $\Psi(\boldsymbol{r})$ constrains $u(r)$ and $w(r)$ by the relation,

$$\int_0^\infty dr \left(u(r)^2 + w(r)^2 \right) = 1, \tag{2.3}$$

with probability that the deuteron is in the $L = 2$ state, denoted by P_D, given by

$$P_D = \int_0^\infty dr \; w(r)^2. \tag{2.4}$$

At distances much larger than the typical nuclear interaction range the radial

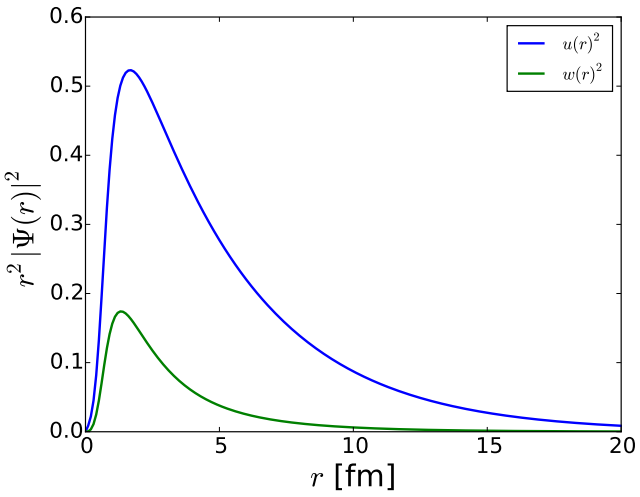

Figure 2.1: The deuteron S and D wave component density distribution as computed with the AV18 potential. The details of the calculation are explained in the results section.

wave functions of the deuteron assume the following asymptotic forms [25],

$$u(r) \to \frac{A_s}{\sqrt{4\pi}} \frac{e^{-\kappa r}}{r}, \tag{2.5}$$

$$w(r) \to A_D \left(1 + \frac{3}{\kappa r} + \frac{3}{\kappa^2 r^2}\right) e^{-\kappa r}. \tag{2.6}$$

In these expressions, $\kappa = \sqrt{2m_\mu^D E_0}$, where m_μ^D is the reduced mass of the proton-neutron system, and A_s, A_D are the asymptotic normalization constants of the S-states and D-states, respectively. In general, even for few-body nuclei, it is difficult to analytically derive the wave function $\Psi(\boldsymbol{r})$ due to the complexity of the nuclear forces involved. Having a simple analytical form of the wave function for a nucleus would have important practical applications, in direct analogy to the utility of the hydrogen wave function for atoms. Due to the short range nature of the nuclear force, the smallness of the D-state, and the small deuteron binding energy, it is possible to neglect the D-states and approximate the deuteron wave function by the S-wave asymptotic expression in equation (2.5). In the "zero-range approximation",

the D-states are neglected to achieve accurate estimates of important nuclear processes [26, 27, 28, 29]. Because the zero-range approximation was recently used by Friar in calculating the nuclear polarizability corrections [30], we provide here a brief overview of this technique. To include the short range behaviour of the zero-range wave function, the effective range analysis formulated by Bethe [27] must be used. From this analysis, one finds that S-state normalization obeys:

$$A_s = \sqrt{\frac{2\kappa}{1-\kappa\rho_d}}, \tag{2.7}$$

where ρ_d is the effective range parameter of the interaction determined from measurements of low-energy cross sections. The deuteron effective range parameter is $\rho_d = 1.765(2)$ fm [30]. Continuum states can be obtained from the partial wave expansion in scattering theory [31]. At lowest order, these states are given by:

$$\psi_S(r) = \frac{\sin(kr)}{kr} - \frac{a_S}{1+ika_S}\frac{e^{ikr}}{r}, \tag{2.8}$$

where a_S represents either the triplet and singlet scattering lengths that have been determined experimentally to be $a_{S=0} = -23.748(10)$ fm, and $a_{S=1} = 5.4194(20)$ fm [30]. Using these values, it is possible to carry out precise calculations of deuteron properties that involve transitions between the ground state and the excited states.

2.1 The Charge Radius

The charge radius $\langle r_{ch}^2 \rangle_d^{1/2}$ of the deuteron can be determined from electron scattering measurements of the deuteron's electric form factor $G_E(Q^2)$ at low momentum

transfers. The explicit relationship between these two quantities is given by,

$$\langle r_{ch}^2 \rangle_d = \int d^3r \; r^2 \rho(\boldsymbol{r}) = -6 \frac{dG_E}{dQ^2}(Q^2)\bigg|_{Q=0}, \tag{2.9}$$

where $\rho(\boldsymbol{r})$ is the nuclear charge density. The deuteron charge operator can be written as [19],

$$\langle r_{ch}^2 \rangle_d = \langle r_{ch}^2 \rangle_p + \langle r_{ch}^2 \rangle_n + \langle r_{str}^2 \rangle_d + ..., \tag{2.10}$$

where $\langle r_{ch}^2 \rangle_p$ and $\langle r_{ch}^2 \rangle_n$ are the charge radii of the proton and neutron, and the ellipsis refers to higher order terms. The term $\langle r_{str}^2 \rangle_d$ is the deuteron structure radius defined as

$$\langle r_{str}^2 \rangle_d = \int \; d^3r \left(\frac{r}{2}\right)^2 |\psi_d(\boldsymbol{r})|^2 = \int_0^\infty dr \; \left(\frac{r}{2}\right)^2 \left(u(r)^2 + w(r)^2\right). \tag{2.11}$$

2.2 The Electric Quadrupole Moment

The concept of a quadrupole moment arises as a result of the multipole decomposition of the electric field generated by a charge distribution. The leading term of such an expansion yields the quadrupole tensor,

$$Q_{ij} = \int \left(3r_i r_j - \delta_{ij} r^2\right) \rho(\mathbf{r}) d^3r. \tag{2.12}$$

The expectation value of the diagonal element Q_{33} on the ground state wave function in the direction of the maximum projection defines the quadrupole moment of a nucleus. For the deuteron, we have

$$Q_d = \langle J_0; J_0 | 3z^2 - r^2 | J_0; J_0 \rangle = \sqrt{\frac{16\pi}{5}} \langle J_0; J_0 | r^2 Y_0^2(\hat{r}) | J_0; J_0 \rangle, \tag{2.13}$$

$$= \frac{1}{\sqrt{50}} \int_0^\infty r^2 \left(u(r)w(r) - \frac{1}{\sqrt{8}} w(r)^2 \right). \tag{2.14}$$

The quadrupole moment is a measure of the sphericity of a nucleus in its ground state, with a non-zero value indicating a departure from spherical symmetry. For the deuteron the non-zero value of Q_d, as shown in Table 2.1, is a result of the small D-state admixture in its ground state, which is due to the tensor force acting between the proton and neutron [32].

2.3 The Magnetic Dipole Moment

The final deuteron static property that we consider is the magnetic dipole moment. The magnetic dipole moment operator is the expectation value of the magnetic dipole moment on the ground state. This operator is defined as,

$$\boldsymbol{M}1 = \mu_N \sum_{i=1}^{A} \left(g_{s_i} \boldsymbol{S}_i + g_{\ell_i} \boldsymbol{\ell}_i \right), \tag{2.15}$$

where we have,

$$g_{s_i} = g_p \hat{p}_i + g_n \hat{n}_i, \qquad g_{\ell_i} = \hat{p}_i, \tag{2.16}$$

$$\hat{p}_i = \frac{(1+\tau_i^3)}{2}, \qquad \hat{n}_i = \frac{(1-\tau_i^3)}{2}, \tag{2.17}$$

τ_i^3 are the z-component isospin projection operators and $g_p = 5.586$, $g_n = -3.826$ are the dimensionless anomalous g-factors of the proton and neutron. Taking the $\hat{z}$ projection of the magnetic dipole operator and computing its expectation value of the deuteron ground state with maximum projection will give:

$$M1 = \frac{(g_p + g_n)}{2} + \frac{3}{4}\left(1 - (g_p + g_n)\right) P_D. \tag{2.18}$$

The deuteron ground state properties defined in this section will be computed and compared to experiment in the results section.

2.4 Nuclear Forces

The description of nucleon-nucleon interactions is one of the central problems in nuclear physics. Within the framework of the standard model, the force binding nucleons together is the strong force. This force is described by the theory of Quantum Chromodynamics, a non-abelian gauge theory possessing SU(3) colour symmetry whose degrees of freedom are quarks and gluons. In principal the interactions between protons and neutrons, which are low energy bound states of three quarks, should admit a full description in terms the underlying quark-quark dynamics. However, due to asymptotic freedom, at energy scales of less than 1 GeV the QCD coupling constant becomes greater than unity and consequently the theory does not admit perturbative analysis. Since the quark degrees of freedom only become important at short distances and high energies, they are not optimal for the description of nuclear structure. Instead we should use the more effective degrees of freedom which are mesons and nucleons.

The first attempt to describe nuclear forces in terms of meson exchange can be traced to the work of Yukawa. In 1935 he proposed that the nuclear force arose due to the exchange of a heavy particle between the nucleons [33] as illustrated in Fig. 2.2. This particle was eventually discovered and called the pion (π). Because of its light mass, it is only suited for describing nuclear forces at distances greater than $\approx$ 2 fm. Shortly after Yukawa's proposal, more sophisticated meson exchange models were used that included pions and scalar and vector mesons such as the ω, ρ, and σ particles [34].

These models contained basic properties of the NN-potential (V_{NN}) such as the

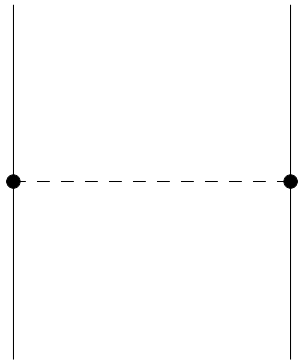

Figure 2.2: The one pion exchange diagram for the nucleon-nucleon force. Nucleons are represented by solid lines, dashed lines are for the pions.

hard core repulsion, an intermediate range attraction, and the long range one-pion-exchange force. The most general set of conditions that must be satisfied by a NN-potential are outlined in Ref. [35]. These conditions are,

- Translational Invariance $\rightarrow V(\boldsymbol{r}_1, \boldsymbol{r}_2) = V(\boldsymbol{r})$,
- Galilean Invariance $\rightarrow V(\boldsymbol{p}_1, \boldsymbol{p}_2) = V(\boldsymbol{p})$,
- Rotational Invariance,
- Parity Invariance $\rightarrow V(\boldsymbol{\sigma}_1, \boldsymbol{\sigma}_2, \boldsymbol{p}, \boldsymbol{r}) = V(\boldsymbol{\sigma}_1, \boldsymbol{\sigma}_2, -\boldsymbol{p}, -\boldsymbol{r})$,
- Time Reversal Invariance,
- Invariance under interchange of two particles $\rightarrow V(\sigma_1, \sigma_2, \boldsymbol{p}, \boldsymbol{r}) = V(\boldsymbol{\sigma}_2, \boldsymbol{\sigma}_1, -\boldsymbol{p}, -\boldsymbol{r})$,
- Approximate Isospin Symmetry $\rightarrow V(\boldsymbol{\tau}_1, \boldsymbol{\tau}_2) = V_1 + (\boldsymbol{\tau}_1 \cdot \boldsymbol{\tau}_2)V_2$,
- Hermicity $\rightarrow V(\boldsymbol{\sigma}_1, \boldsymbol{\sigma}_2, \boldsymbol{p}, \boldsymbol{r}) = V^{\dagger}(\boldsymbol{\sigma}_1, \boldsymbol{\sigma}_2, \boldsymbol{p}, \boldsymbol{r})$.

Here, $\boldsymbol{\sigma}_{1,2}$ are the usual Pauli matrices and $\boldsymbol{p} = \frac{\boldsymbol{p}_2 - \boldsymbol{p}_1}{2}$, $\boldsymbol{r} = \boldsymbol{r}_2 - \boldsymbol{r}_1$ are the relative momenta and radial coordinates. Any realistic description of the NN force must satisfy these basic properties.

2.5 The AV18 Nuclear Potential

One of the most accurate and widely used two-body nuclear potentials is the AV18 potential [36]. This potential can be broken down into the sum of three terms,

$$V^{NN} = V_{EM}^{NN} + V_{\pi}^{NN} + V_{R}^{NN}, \tag{2.19}$$

Where V_{π}^{NN} is the pion exchange term, V_{EM}^{NN} is the electromagnetic term (mostly Coulomb), and V_{R}^{NN} is the short and intermediate range term of the potential. The electromagnetic component of the nucleon-nucleon potential is obtained from the non-relativistic reduction of a two particle wave function and depends on which two interacting particles are being considered.

Based on the constraints in the earlier list, the most general set of operators $\hat{O}_{R}^{NN}$ that can contribute to the short and intermediate range V_{R}^{NN} component of the nucleon-nucleon force, up to terms quadratic in momentum, is given by,

$$\hat{O}_{R}^{NN} = \{1, \boldsymbol{\sigma}_1 \cdot \boldsymbol{\sigma}_2, \hat{L}^2, (\boldsymbol{\sigma}_1 \cdot \boldsymbol{\sigma}_2)\,\hat{L}^2, S_{12}, \hat{L} \cdot \hat{S}, (\hat{L} \cdot \hat{S})^2\} \otimes \{1, \boldsymbol{\tau}_1 \cdot \boldsymbol{\tau}_2\}, \tag{2.20}$$

$\boldsymbol{\sigma}_1$, $\boldsymbol{\sigma}_2$ are the spin of the first and second nucleon, and $S_{12} = 3(\boldsymbol{\sigma}_1 \cdot \hat{r})(\boldsymbol{\sigma}_2 \cdot \hat{r}) - \boldsymbol{\sigma}_1 \cdot \boldsymbol{\sigma}_2$, the tensor force. In addition to these 14-terms, there are four additional charge-breaking operators that are included into the potential of the form,

$$\hat{O}_{R}^{NN} = \{T_{12}, (\boldsymbol{\sigma}_1 \cdot \boldsymbol{\sigma}_2)T_{12}, S_{12}T_{12}, (\tau_{z_1} + \tau_{z_2})\} \tag{2.21}$$

where $T_{12} = 3\tau_{z_1}\tau_{z_2} - \boldsymbol{\tau}_1 \cdot \boldsymbol{\tau}_2$ is the isotensor operator. The V_R potential can then be written as a sum of these 18-terms,

$$V_R^{NN} = \sum_{i=1}^{18} v_{i,ST}^{NN}(r)\hat{O}_{R,i}^{NN}. \tag{2.22}$$

Each of the terms $v_{i,ST}^{NN}(r)$ consists of a function having the range of a two-pion exchange force and a Wood-Saxon potential multiplied by a second degree polynomial of the radial coordinate r. This potential is constrained by first determining the depth and range parameters of the Wood-Saxon potential and the one pion exchange cut off. After this initial fitting, the remaining parameters were fit to the Nijmegen nucleon-nucleon phase shifts [36] and produced a total χ^2 per datum of 1.34 for the energy range between $2 - 350$ MeV.

2.6 Chiral Perturbation Theory

The modern technique to derive the nucleon-nucleon force comes from chiral effective field theory (χ_{EFT}). χ_{EFT} is the low-energy approximation to QCD originally proposed by Steven Weinberg in his seminal papers [37, 38]. The advantage of this approach, is that an effective Lagrangian describing the nucleon-nucleon interaction can be Taylor expanded in powers ν of the ratio Q/Λ_χ, where Q is the soft scale of the theory, roughly the pion mass, and Λ_χ is the chiral symmetry breaking scale, roughly 1 GeV.

The QCD Lagrangian is,

$$\mathcal{L}_{QCD} = \sum_f \bar{q}_f \left(i\not{\mathcal{D}} - m_f\right) q_f - \frac{1}{4}\mathcal{G}_{a,\mu\nu}\mathcal{G}_a^{\mu\nu}, \tag{2.23}$$

where the summation is over quark flavours, q_f denotes the quark fields, m_f the quark masses and the covariant derivative $\mathcal{D}_\mu$ is,

$$\mathcal{D}_\mu = \partial_\mu - ig\frac{\lambda_a}{2}\mathcal{A}_{\mu,a}. \tag{2.24}$$

Here, $\mathcal{A}_{\mu,a}$ are the gluon fields, λ_a are the Gell-Mann matrices and g is the strong coupling constant. The gluon color field strength tensor $\mathcal{G}_{a,\mu\nu}$ is given by,

$$\mathcal{G}_{a,\mu\nu} = \partial_\mu \mathcal{A}_{\nu,a} - \partial_\nu \mathcal{A}_{\mu,a} + g f_{abc}\mathcal{A}_{\mu,b}\mathcal{A}_{\nu,c}. \tag{2.25}$$

The indices a, b, c run over the dimensions of the $SU(3)_{\text{color}}$ Lie algebra and f_{abc} are its structure constants.

The two lightest quarks, u, d, which compose the nucleons (proton (uud), neutron (udd)) have masses $m_u \sim 2.3$ MeV, $m_d \sim 4.8$ MeV which are much smaller than typical hadronic scales. Therefore, we will consider the $\mathcal{L}_{QCD}$ in the limit of vanishing quark masses for these two flavours. In this limit we have,

$$\lim_{m_u, m_d \to 0} \mathcal{L}_{QCD} = i\bar{q}_R \not{\mathcal{D}} q_R + i\bar{q}_L \not{\mathcal{D}} q_L - \frac{1}{4}\mathcal{G}_{a,\mu\nu}\mathcal{G}_a^{\mu\nu} \tag{2.26}$$

where $q_R = P_R q$, $q_L = P_L q$ are the right and left handed projections of the quark fields and the projection operators P_R, P_L are defined as,

$$P_R = \frac{1}{2}\left(1 + \gamma_5\right), \tag{2.27}$$

$$P_L = \frac{1}{2}\left(1 - \gamma_5\right). \tag{2.28}$$

This Lagrangian is then invariant under the unitary transformations $q_L \to e^{-\frac{i}{2}\boldsymbol{\theta}_L \cdot \boldsymbol{\tau}}$ and $q_R \to e^{-\frac{i}{2}\boldsymbol{\theta}_R \cdot \boldsymbol{\tau}}$, where $\boldsymbol{\tau}$ are the generators of $SU(2)_{\text{flavour}}$ (,*i.e.*, the Pauli matrices $(\tau_1, \tau_2, \tau_3) = \boldsymbol{\tau}$). This property of $\mathcal{L}_{QCD}$ in the limit of vanishing quark masses is

known as chiral symmetry. Chiral symmetry is broken explicitly by the small, but non-zero, masses of the quarks, and also spontaneously. The spontaneous chiral symmetry breaking occurs because chiral symmetry is not realized in the ground state of the theory. The strongest evidence comes from the hadron mass spectrum. For example, the rho meson (ρ) which has a spin and parity ($J^\pi = 1^-$) differs in mass from the ($J^\pi = 1^{+)}$ meson (a_1) by 454 MeV and so is not degenerate with it. However, the three charged states of the rho meson ($\rho^{\{+,-,0\}}$) differ in mass by only a few MeV. Therefore, we see that the hadron spectrum obeys isospin symmetry ($SU(2)_V$), but the axial symmetry is broken. This spontaneous symmetry breaking of the Lagrangian implies the existence of goldstone bosons, identified here as the pions.

Using nucleons and pions as the relevant degrees of freedom, the most general Lagrangian is then constructed by imposing chiral symmetry as an additional symmetry to those mentioned in section 2.4. For the theory to be tractable, a power counting prescription must be employed to classify nuclear interactions from most to least dominant, containing a finite number of terms at each order. The conventional method to classify the order of a Feynman diagram in this theory is given by Weinberg [37] as,

$$\nu = -4 + 2A + 2L + \sum_i \Delta_i, \tag{2.29}$$

where A is the number of nucleons, L is the number of loops, the sum runs over all vertices i in the diagram, and Δ_i is defined as,

$$\Delta_i = (d_i + \frac{n_i}{2} - 2). \tag{2.30}$$

Here, d_i is the number of pion mass insertions, and n_i is the number of nucleon fields

involved in the vertex i. For example, in the one pion exchange depicted in Figure 2.2 we have the number of nucleons A=2, the number of loops L=0, and $d_i = 0$, $n_i = 2$ for $i = 1, 2$. Therefore, the order of this diagram is $\nu = 0$.

Using this power counting prescription, the effective Lagrangian can then be Taylor-expanded in powers of the chiral order ν,

$$\mathcal{L}_{QCD} = \sum_{\nu} \left(\frac{Q}{\Lambda_\chi} \right)^{\nu} \mathcal{L}_{N^\nu LO}. \tag{2.31}$$

At each order in the expansion a finite set of constants $\{c_i\}$ will be introduced that must be fitted to nucleon-nucleon phase shifts or Nijmegen partial wave analysis. This expansion converges when $Q/\Lambda_\chi \ll 1$, allowing nuclear forces to be modelled to the desired level of accuracy. The hierarchy of the nuclear forces emerging from this power counting prescription is shown in Figure 2.3.

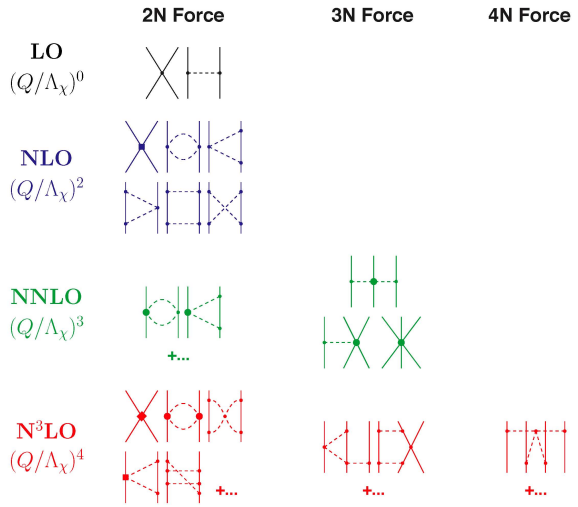

Figure 2.3: Hierarchy of nuclear forces in χ_{EFT} [39].

Because χ_{EFT} is valid only up to energy scales below $\Lambda_\chi \sim 1$ GeV, a regulator must be used to suppress high momentum contributions in calculations of Feynman

amplitudes. The regulator depends on an energy scale Λ to enforce this constraint. The most commonly employed regulator is of the form,

$$F(\Lambda, p, p') = \text{Exp}\left[-\left(\frac{p}{\Lambda}\right)^{2n} - \left(\frac{p'}{\Lambda}\right)^{2n}\right], \tag{2.32}$$

where the exponent n is chosen to minimize effects on the nuclear forces at a given chiral order. These potentials are then applied to a Lippmann-Schwinger equation to obtain the T-matrix elements from which observables are calculated.

In this work, the χ_{EFT} potentials that we will use are the N^{3}LO potential of Entem and Machleidt [40] (N^{3}LO-EM) and the N^{k}LO potentials developed by Epelbaum *et al* [40]. The N^{3}LO potential of Entem and Machleidt employed dimensional regularization with a fixed cut off of $\Lambda = 500$ MeV to regulate the Lippmann-Schwinger equation. At low energies, the χ^2/datum for this potential was ~ 1.05. The Epelbaum *et al.* potentials employed two categories of integration cut off's: one which enters the Lippmann-Schwinger equation (Λ) and one to regulate the two pion exchange ($\tilde{\Lambda}$). The exact cut off values that were used will be mentioned in Chapter 4.

Chapter 3

Nuclear Structure Corrections to the Lamb Shift in Muonic Atoms

The Hamiltonian of a non-relativistic lepton and a nucleus of charge $-e$ and Ze, respectively, interacting through a Coulomb force in the center of mass frame, illustrated for muonic deuterium in Fig 3.1, is given by:

$$\hat{H}_\mu = \frac{q^2}{2m_r} - \frac{Z\alpha}{r}, \tag{3.1}$$

where m_r is the reduced mass in the nucleus-lepton center of mass system and r is the relative distance between the muon and the center of mass of the nucleus. Solving the Schrödinger equation for the bound states will give us the Bohr energy levels and wave functions:

$$\varepsilon_n = -\frac{m_r(Z\alpha)^2}{2n^2}, \tag{3.2}$$

$$\phi_{n\ell m}(r) = \sqrt{\frac{4\pi}{2\ell+1}}\phi_n(0)R_{n\ell}\left(\frac{m_r Z\alpha}{n}r\right)Y_m^\ell(\hat{r}), \tag{3.3}$$

$$\phi_n^2(0) = \frac{(m_r Z\alpha)^3}{n^3\pi}. \tag{3.4}$$

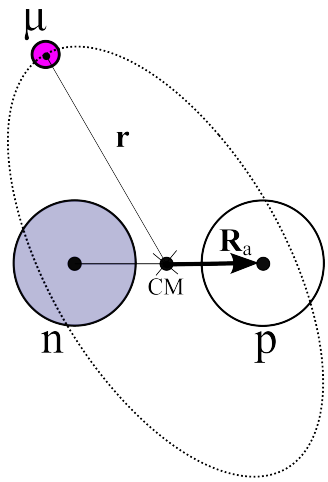

Figure 3.1: Coordinates in muonic deuterium. The figure is not to scale.

Here, n is the principal quantum number and ℓ is the angular momentum. Each energy level has a degeneracy of n with respect to the orbital angular momentum ℓ and $2\ell+1$ for the magnetic quantum number m. The few wave-functions in the n=2 states are,

$$R_{20}\left(\frac{m_r Z\alpha}{2}r\right) = \left(1 - \frac{m_r Z\alpha r}{2}\right) e^{-\frac{m_r Z\alpha}{2}r}, \tag{3.5}$$

$$R_{21}\left(\frac{m_r Z\alpha}{2}r\right) = \frac{m_r Z\alpha r}{2} e^{-\frac{1}{2}m_r Z\alpha r}. \tag{3.6}$$

The relativistic hydrogenic system may be treated through the use of the Dirac Hamiltonian in the infinite nuclear mass limit. In this limit, the Dirac-Coulomb Hamiltonian is given by:

$$H_{DC} = \boldsymbol{\alpha}\cdot\boldsymbol{p} + \beta m - \frac{Z\alpha}{r}. \tag{3.7}$$

Solving this equation for the energy levels will result in [41]:

$$E_{n,j} = m\left(1 + \frac{1}{\sqrt{1 + \frac{(Z\alpha)^2}{\left(n-j-\frac{1}{2}+\sqrt{(j+\frac{1}{2})^2-(Z\alpha)^2}\right)^2}}}\right)^{-1/2}. \tag{3.8}$$

The lepton spin and angular momentum coupling in the Dirac-Coulomb Hamiltonian has lifted some of the degeneracies of the Bohr energy levels with $j = \ell \pm 1/2$. However, this equation does not generate the splitting between the $2S_{\frac{1}{2}}$ and $2P_{\frac{1}{2}}$ states. The measured energy difference between the $2S$ and $2P$ energy levels is known as the Lamb shift. The Lamb shift of muonic deuterium (μD) is shown in Fig 3.2. The most dominant sources of the Lamb shift are the δ_{QED} corrections in equation (1.1). Different groups have calculated these corrections and are in agreement Ref. [17]. A thorough review of this subject can be found in Refs. [42, 43].

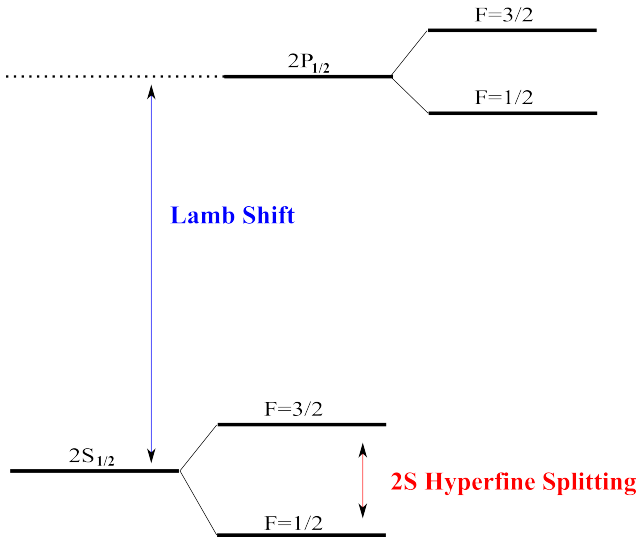

Figure 3.2: The Lamb Shift in muonic deuterium. The figure is not to scale.

As discussed in Chapter 1, nuclear structure effects also contribute to the Lamb shift splitting. These nuclear structure corrections can be separated into two distinct components, the elastic and inelastic contributions. The former neglects the excitations of the nucleus, while the inelastic contributions take them into account. The precise treatment of these corrections will occupy our discussions for the rest of the Chapter.

3.1 Elastic Corrections

The elastic contributions arise from the finite nuclear size where the nucleus stays in the ground state. Some of the earliest work to consider these effects is from Karpus *et al.* [44]. A more rigorous derivation was performed by Friar [45] using first, second and third order perturbation theory and considering all corrections up to $(Z\alpha)^6$. To calculate these elastic contributions, we consider the following non-relativistic Hamiltonian describing our muonic system,

$$\hat{H} = \hat{H}_\mu + \Delta H, \tag{3.9}$$

where $\hat{H}_\mu$ describes the muon's interaction with a point-like Coulomb source in the center of mass frame as in equation (3.1) and ΔH is the finite nuclear size correction,

$$\Delta H = \int d\boldsymbol{s}\ \rho(\boldsymbol{s}) \Delta V(\boldsymbol{r}, \boldsymbol{s}) \tag{3.10}$$

$$\Delta V(\boldsymbol{r}, \boldsymbol{s}) = Z\alpha \left(\frac{1}{r} - \frac{1}{|\boldsymbol{r} - \boldsymbol{s}|} \right), \tag{3.11}$$

where $\rho(\boldsymbol{s})$ is the normalized nuclear charge density. Using the non-relativistic hydrogenic wave function and the Coulomb Green's function [45, 46], Friar determined that the non-relativistic energy corrections up to fifth order in $(Z\alpha)$ for the $2S$-states are given by:

$$\Delta E_{NR} = \frac{2\pi(Z\alpha)}{3} |\phi_n(0)|^2 \langle r_{ch}^2 \rangle + \delta_{Zem}. \tag{3.12}$$

The second term in this equation is the third Zemach moment, defined as a convolution over the nuclear charge density, $\rho_E(\boldsymbol{R})$,

$$\delta_{Zem} = -\frac{m_r^4}{24} (Z\alpha)^5 \int d\boldsymbol{R} \int d\boldsymbol{R}'\ |\boldsymbol{R} - \boldsymbol{R}'|^n \rho_E(\boldsymbol{R}) \rho_E(\boldsymbol{R}'). \tag{3.13}$$

To calculate the relativistic corrections Friar used the Dirac wave-function in conjunction with the Dirac-Coulomb propagator. These relativistic corrections contribute at orders higher than 5^{th} order and are consequently neglected in our calculation.

3.2 Inelastic Corrections

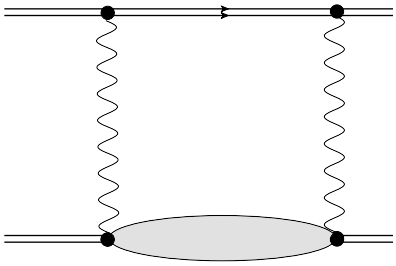

Figure 3.3: Non-relativistic two-photon exchange diagram.

Having discussed the elastic contributions, we wish to account for the non-relativistic effects of nuclear excitations on the Lamb shift in muonic atoms. These inelastic contributions are represented diagrammatically by the two-photon exchange process illustrated in Figure 3.3. This energy contribution to the Lamb shift is of order $(Z\alpha)^5$. The non-relativistic Hamiltonian in the center of mass frame describing our muonic atom is given by:

$$\hat{H} = \hat{H}_\mu + \hat{H}_N - \Delta H, \tag{3.14}$$

where H_μ is given by equation (3.1) and ΔH is defined as,

$$\Delta H = \sum_a^Z \Delta V(\boldsymbol{r}, \boldsymbol{R}_a), \tag{3.15}$$

$$\Delta V = \alpha \left(\frac{1}{|\boldsymbol{r} - \boldsymbol{R}_a|} - \frac{1}{r} \right). \tag{3.16}$$

The new addition to the Hamiltonian is the nuclear Hamiltonian $\hat{H}_N$ which consists the of kinetic energy and the nuclear potential, discussed in Chapter 2.

We now introduce the transition proton density operator,

$$\rho_N(\boldsymbol{R}) = \frac{1}{Z}\langle N|\sum_a^Z \delta(\boldsymbol{R}-\boldsymbol{R}_a)|N_0\rangle. \tag{3.17}$$

This allows the sum of matrix elements $\sum_a^Z \langle N|\Delta V(\boldsymbol{r},\boldsymbol{R})|N_0\rangle$ to be written as,

$$\sum_a^Z \langle N|\Delta V(\boldsymbol{r},\boldsymbol{R})|N\rangle = Z\int d\boldsymbol{R}\ \rho_N(\boldsymbol{R})\Delta V(\boldsymbol{r},\boldsymbol{R}). \tag{3.18}$$

The energy corrections due to nuclear structure are obtained in the non-relativistic limit from second order perturbation theory,

$$\delta_{NR} = \langle N_0\mu_0|\Delta H\hat{G}\Delta H|N_0\mu_0\rangle, \tag{3.19}$$

where $\hat{G}$ is the Green's function for our Hamiltonian,

$$\hat{G}(E_0,\varepsilon_{\mu_0}) = \frac{1}{E_0+\varepsilon_{\mu_0}-H_\mu-H_N}. \tag{3.20}$$

The energy E_0 is the ground state energy of the muon, while ε_{μ_0} is the binding energy of the muon in the $n=2$ state. Inserting the coordinate space completeness relation minus the ground state, $1-|N_0\rangle\langle N_0| = \sum_{N\neq N_0}|N\rangle\langle N|$, and using equation (3.18), we have,

$$\delta_{NR} = -\sum_{N\neq N_0}\int d\boldsymbol{R}\int d\boldsymbol{R}'\rho_N^*(\boldsymbol{R})P_{NR}(\boldsymbol{R},\boldsymbol{R}',\omega_N)\rho_N(\boldsymbol{R}'), \tag{3.21}$$

where

$$P_{NR}(\boldsymbol{R},\boldsymbol{R}',\omega_N) = -Z^2\int d\boldsymbol{r}\int d\boldsymbol{r}'\Delta V(\boldsymbol{r},\boldsymbol{R})\langle\mu_0|\boldsymbol{r}\rangle\langle\boldsymbol{r}|\frac{1}{H_\mu+\omega_N-\varepsilon_{\mu_0}}|\boldsymbol{r}'\rangle\langle\boldsymbol{r}'|\mu_0\rangle\Delta V(\boldsymbol{r}',\boldsymbol{R}'). \tag{3.22}$$

Here, we have introduced the nuclear excitation energy $\omega_N = E_N - E_0$, where $\hat{H}_N|N\rangle = E_N|N\rangle$. For convenience, we will write $\phi(0)$ in place of $\phi_2(0)$, so that $\phi^2(0) = (m_r Z\alpha)^3/(8\pi)$.

The corrections at fifth order in $Z\alpha$ are obtained by approximating the muon wave-function and propagator to leading order:

$$R_{20}\left(\frac{m_r Z\alpha}{2}r\right) \approx 1, \qquad \varepsilon_{\mu_0} \approx 0, \tag{3.23}$$

$$R_{21}\left(\frac{m_r Z\alpha}{2}r\right) \approx 0, \qquad H_\mu \approx \frac{q^2}{2m_r}. \tag{3.24}$$

Using these approximations, the energy correction to the $2P$ level vanishes. For the $2S$ states, we have that P_{NR} is diagonal in the momentum basis,

$$P_{NR} = -\phi^2(0)Z^2 \int \frac{d^3q}{(2\pi)^3}\left(\frac{4\pi\alpha}{q^2}\right)^2 \frac{1}{\frac{q^2}{2m_r}+\omega_N}(1-e^{i\boldsymbol{q}\cdot\boldsymbol{R}})(1-e^{-i\boldsymbol{q}\cdot\boldsymbol{R}'}). \tag{3.25}$$

Expanding out the product of the exponentials and integrating over the angular part, we obtain:

$$P_{NR} = -16m_r(Z\alpha)^2\phi^2(0)\int_0^\infty dq \frac{\left(1-\frac{\sin(qR)}{qR}-\frac{\sin(qR')}{qR'}+\frac{\sin(q|\boldsymbol{R}-\boldsymbol{R}'|)}{q|\boldsymbol{R}-\boldsymbol{R}'|}\right)}{q^2\left(q^2+2m_r\omega_N\right)}. \tag{3.26}$$

Upon reinserting the completeness of nuclear states, we find that terms that depend only on one coordinate $\boldsymbol{R}$ or $\boldsymbol{R}'$ do not contribute to the energy shift. Such terms give matrix elements of the form $\langle N|f(\boldsymbol{R})|N_0\rangle\langle N|N_0\rangle$, which is zero due to the orthogonality of the nuclear states $|N\rangle$ and $|N_0\rangle$. Therefore, the only relevant term in the above expression is,

$$P_{NR}(\boldsymbol{R},\boldsymbol{R}',\omega_N) = -16m_r\alpha^2Z^2\phi^2(0)\int_0^\infty dq \frac{\left(\frac{\sin(q|\boldsymbol{R}-\boldsymbol{R}'|)}{q|\boldsymbol{R}-\boldsymbol{R}'|}-1\right)}{q^2\left(q^2+2m_r\omega_N\right)}, \tag{3.27}$$

which can be evaluated analytically to yield:

$$P_{NR} = -\frac{2\pi\alpha^2 Z^2 \phi^2(0)}{m_r \omega_N^2} \frac{1}{|\boldsymbol{R}-\boldsymbol{R}'|} \cdot \left[e^{-\sqrt{2m_r\omega_N}|\boldsymbol{R}-\boldsymbol{R}'|} - 1 + \sqrt{2m_r\omega_N}|\boldsymbol{R}-\boldsymbol{R}'| - \omega_N m_r |\boldsymbol{R}-\boldsymbol{R}'|^2 \right]. \quad (3.28)$$

Here, $|\boldsymbol{R}-\boldsymbol{R}'|$ is the virtual distance that the protons travel during the two-photon exchange process. To estimate the magnitude of this quantity, we consider the momentum scale related to the nuclear excitation during the two-photon exchange as $\sqrt{2m_N\omega_N}$. By the uncertainty principle we obtain:

$$|\boldsymbol{R}-\boldsymbol{R}'| \approx \frac{1}{\sqrt{2m_N\omega_N}}, \quad (3.29)$$

which, in the case of the deuteron implies,

$$\sqrt{2m_r\omega_N}|\boldsymbol{R}-\boldsymbol{R}'| \approx \sqrt{\frac{m_r}{m_N}} < 1. \quad (3.30)$$

The small size of this parameter guarantees that the expansion of $P_{NR}(\boldsymbol{R}, \boldsymbol{R}', \omega_N)$ as a power series in $\sqrt{2m_r\omega_N}|\boldsymbol{R}-\boldsymbol{R}'|$ converges. The first three terms in the expansion are given by:

$$P_{NR} = \frac{2\pi}{3}(Z\alpha)^2\phi^2(0)\sqrt{\frac{2m_r}{\omega_N}} \left[|\boldsymbol{R}-\boldsymbol{R}'|^2 - \frac{1}{4}|\boldsymbol{R}-\boldsymbol{R}'|^3 - \frac{1}{10}m_r\omega_N|\boldsymbol{R}-\boldsymbol{R}'|^4 \right]. \quad (3.31)$$

The terms in even powers of $|\boldsymbol{R}-\boldsymbol{R}'|$ can be expanded in terms of spherical harmonics by making use of the following expressions:

$$|\boldsymbol{R}-\boldsymbol{R}'|^2 \to -\frac{8\pi}{3} R R' \sum_m Y_m^{1*}(\hat{R}) Y_m^1(\hat{R}'), \quad (3.32)$$

$$|\boldsymbol{R}-\boldsymbol{R}'|^4 \to \frac{10}{3}R^2R'^2 - \frac{16\pi}{3}(R^2+R'^2)RR'\sum_m Y_m^1(\hat{R})Y_m^{1*}(\hat{R}') + \frac{32\pi}{15}R^2R'^2\sum_{m'}Y_{m'}^2(\hat{R})Y_{m'}^{2*}(\hat{R}'). \quad (3.33)$$

Inserting equation (3.32) into the energy correction in equation (3.21), using the definition of $\rho_N(\boldsymbol{R})$ in equation (3.17), and with the aid of the Wigner-Eckart theorem in Appendix A, we obtain the leading order dipole correction [47],

$$\delta_{D1}^{(0)} = -\frac{16\pi^2}{9}\phi^2(0)(Z\alpha)^2 \int\limits_{\omega_{th}}^{\infty} d\omega \sqrt{\frac{2m_r}{\omega_N}} S_{\hat{D}_1}(\omega). \tag{3.34}$$

Here we define the dipole operator $\hat{D}_1$ and its response function $S_{\hat{D}_1}(\omega)$ by:

$$\hat{D}_1 = \frac{1}{Z}\sum_a^A \hat{e}_a R_a Y^a(\hat{R}_a), \tag{3.35}$$

$$S_{\hat{D}_1}(\omega) = \frac{1}{2J_0+1}\sum_{N\neq N_0,J} |\langle N_0 J_0||\hat{D}_1||NJ\rangle|^2 \delta(\omega_N - \omega), \tag{3.36}$$

Where, $\hat{e}_a$ is the charge projection operator of the a^{th} nucleon, and $\langle N_0 J_0||\hat{D}_1||NJ\rangle$ indicates the reduced matrix elements, as defined in Appendix A.

The second term in equation (3.31) is energy independent, hence it can be cast into the following form, using $\sum\limits_{N\neq N_0} |N\rangle\langle N| = 1 - |N_0\rangle\langle N_0|$,

$$\delta^{(1)} = \delta_{R3pp}^{(1)} + \delta_{Z3}^{(1)}, \tag{3.37}$$

with,

$$\delta_{R3pp}^{(1)} = -\frac{\pi\alpha^2 Z^2}{3} m_r \phi^2(0) \int d\boldsymbol{R} \int d\boldsymbol{R}'\ |\boldsymbol{R}-\boldsymbol{R}'|^3 \rho_0^{(2)}(\boldsymbol{R},\boldsymbol{R}'), \tag{3.38}$$

$$\delta_{Z3}^{(1)} = \frac{\pi\alpha^2 Z^2}{3} m_r \phi^2(0) \int d\boldsymbol{R} \int d\boldsymbol{R}'\ |\boldsymbol{R}-\boldsymbol{R}'|^3 \rho_0(\boldsymbol{s})\rho_0(\boldsymbol{s}'), \tag{3.39}$$

where

$$\rho_0(\boldsymbol{R}) = \langle N_0|\frac{1}{Z}\sum_a \delta(\boldsymbol{R}-\boldsymbol{R}_a)|N_0\rangle, \tag{3.40}$$

$$\rho_0^{(2)}(\boldsymbol{R}) = \langle N_0|\frac{1}{Z^2}\sum_{ab} \delta(\boldsymbol{R}-\boldsymbol{R}_a)\delta(\boldsymbol{R}-\boldsymbol{R}_b)|N_0\rangle. \tag{3.41}$$

Here, $\rho^{(2)}(\boldsymbol{R}, \boldsymbol{R}')$ is the proton-proton correlation function and $\rho_0(\boldsymbol{R})$ coincides with $\rho_E(\boldsymbol{R})$ in the point-nucleon limit. For the deuteron, where $Z = 1$, the charge correlation contribution function vanishes. The term in equation (3.39) is third Zemach moment that appeared in the elastic contributions in equation (3.12) but with opposite sign, leading to a cancellation of both terms. This cancellation has been noted before in Refs. [30, 20].

In manner analogous to the derivation of $\delta^{(0)}_{D1}$ we insert equation (3.33) into equation (3.21) and using the Wigner-Eckart theorem we obtain the energy correction $\delta^{(2)}$ to the Lamb shift as:

$$\delta^{(2)} = \delta^{(2)}_{R2} + \delta^{(2)}_{Q} + \delta^{(2)}_{D1D3}, \tag{3.42}$$

where $\delta^{(2)}_{R2}$ is the monopole correction, $\delta^{(2)}_{Q}$ the quadrupole, and $\delta^{(2)}_{D1D3}$ is the dipole interference term. These energy corrections are

$$\delta^{(2)}_{R2} = \frac{2\pi}{15} m_r^2 (Z\alpha)^2 \phi^2(0) \left(\frac{10}{3}\right) \int_0^\infty d\omega \sqrt{\frac{\omega}{2m_r}} S_{R^2}(\omega), \tag{3.43}$$

$$\delta^{(2)}_{Q} = \frac{2\pi}{15} m_r^2 (Z\alpha)^2 \phi^2(0) \left(\frac{32\pi}{15}\right) \int_0^\infty d\omega \sqrt{\frac{\omega}{2m_r}} S_{Q_2}(\omega), \tag{3.44}$$

$$\delta^{(2)}_{D1D3} = -\frac{2\pi}{15} m_r^2 (Z\alpha)^2 \phi^2(0) \left(\frac{32\pi}{3}\right) \int_0^\infty d\omega \sqrt{\frac{\omega}{2m_r}} S_{D_1 D_3}(\omega). \tag{3.45}$$

The operators in the response functions are

$$R^2 = \frac{1}{Z}\sum_a^Z R_a^2, \tag{3.46}$$

$$Q_2 = \frac{1}{Z}\sum_a^Z R_a^2 Y_2(\hat{R}_a), \tag{3.47}$$

$$D_3 = \frac{1}{Z}\sum_a^Z R_a^3 Y_1(\hat{R}_a), \tag{3.48}$$

$$D_1 + D_3 = \frac{1}{Z}\sum_a^Z (R_a^3 + R_a) Y_1(\hat{R}_a). \tag{3.49}$$

The dipole interference response function is defined as

$$S_{D_1 D_3}(\omega) = \frac{1}{2}\left(S_{D_1+D_3}(\omega) - S_{D_1}(\omega) - S_{D_3}(\omega)\right). \tag{3.50}$$

3.2.1 Coulomb Distortion Effects

In the previous section, we neglected the effects of the Coulomb interactions between the nucleus and the intermediate muon states by using the free muon propagator in Figure 3.3. To account for these higher order, non-relativistic effects we use the full Coulomb Green's function $G_C(\boldsymbol{r}, \boldsymbol{r}')$ which satisfies,

$$\left(-\omega_N + \frac{1}{2m_r}\boldsymbol{\nabla}^2 + \frac{Z\alpha}{r}\right) G_C(-\omega_N; \boldsymbol{r}, \boldsymbol{r}') = \delta(\boldsymbol{r} - \boldsymbol{r}'). \tag{3.51}$$

The second order correction to the Lamb shift in the hyperfine basis $|NJ, (\ell s)j; FM_F\rangle$ is:

$$\delta_C = \frac{4\pi}{2\ell_0 + 1}\phi^2(0) \int d\boldsymbol{r}' \int d\boldsymbol{r}' \langle \mu_0|\boldsymbol{r}\rangle\langle \mu_0|\boldsymbol{r}'\rangle$$
$$\langle N_0 J_0; F_0 M_{F_0}|\Delta H \hat{G}_C(\omega_N, \varepsilon_{\mu_0}, \boldsymbol{r}, \boldsymbol{r}')\Delta H|N_0 J_0; F_0 M_{F_0}\rangle. \tag{3.52}$$

This Green's function can then be expanded in the hyperfine basis as.

$$G_C(\boldsymbol{r},\boldsymbol{r}') = \sum_{N\neq N_0}\sum_{\ell jJ}\sum_{FM_F} |NJ,(\ell\frac{1}{2})j;FM_F\rangle \frac{g_\ell(\omega_N,r,r')}{rr'} \langle NJ,(\ell\frac{1}{2})j;FM_F|, \quad (3.53)$$

where $g_\ell(\omega_N,r,r')$ is the reduced Coulomb Green's function [46]. Through the introduction of this expansion into the energy correction equation (3.52), in the point nucleon limit, we have:

$$\delta_C = \phi^2(0)\sum_{ab}^{Z}\sum_{\substack{FM_F\\ \ell jJ}}\left(\frac{4\pi\alpha}{3}\right)^2\frac{4\pi}{2\ell_0+1}\int dr\int dr' rr' R_{n\ell_0}(r)R_{n\ell_0}(r')g_\ell(\omega_N,\varepsilon_{\mu_0},r,r')$$

$$\cdot\langle N_0J_0;F_0M_{F_0}|\Delta V(\boldsymbol{r},\boldsymbol{R}_a)|NJ;FM\rangle\langle NJ;FM|\Delta V(\boldsymbol{r}',\boldsymbol{R}_b)|N_0J_0;F_0M_{F_0}\rangle. \quad (3.54)$$

Since $r \gg R_a$ the potential $\Delta V(\boldsymbol{r},\boldsymbol{R}_a)$ can be expanded in terms of multipoles. The leading order correction of this equation, is $\ell = \ell' = 1$, which gives us the leading order Coulomb correction [47]

$$\delta_C^{(0)} = -\frac{16\pi^2}{9}(Z\alpha)^3\phi^2(0)^2\int_{\omega_{th}}^{\infty} d\omega\ \left(\frac{m_r}{\omega}\right)\ln\left(\frac{2(Z\alpha)^2m_r}{\omega}\right)S_{D1}(\omega). \quad (3.55)$$

3.2.2 Relativistic Corrections

We now treat the two photon exchange diagram in a fully covariant fashion. To obtain this energy correction we use the relativistic two-photon propagator. Assuming that the muon acts like a static source and treating it as a free particle, in momentum space, the leading order energy correction is given by [48, 49]:

$$\Delta E = (4\pi\alpha)^2\phi^2(0)\int\frac{d^4q}{(2\pi)^4}D^{\mu\rho}(q)D^{\nu\tau}(-q)t_{\mu\nu}(q,k)T^{\rho\tau}(q,-q), \quad (3.56)$$

$$T^{\rho\tau}(q,-q) = \sum_N \left(\frac{\langle N_0|j^\rho(\boldsymbol{q})|N\rangle\langle N|j^\tau(-\boldsymbol{q})|N_0\rangle}{E_0 - E_n + q_0 + i\epsilon} + \frac{\langle 0|j^\tau(\boldsymbol{q})|N\rangle\langle N|j^\rho(-\boldsymbol{q})|N_0\rangle}{E_0 - E_n - q_0 + i\epsilon}) \right)$$
$$+ \text{Seagull}, \tag{3.57}$$

where $t_{\mu\nu}(q,k)$ is the lepton Compton tensor which has been averaged over initial and final spins, while $T^{\rho\tau}(q,-q)$ is the forward virtual Compton tensor in momentum space. The seagull term is introduced to preserve the Coulomb gauge invariance and keep the integral in equation (3.69) finite [48]. Through straightforward manipulations of the above expressions in the approximation where $k^\mu = (m, \mathbf{0})$, it can be shown that in the Coulomb gauge the energy correction can be written as the sum of the transverse and longitudinal components of the forward virtual Compton amplitude [48]

$$\Delta E = (4\pi\alpha)^2 \text{Im} \int \frac{d^4q}{(2\pi)^4} \frac{2m}{(q^2+i\epsilon)^2 - 4m^2q_0^2} \left(\frac{1}{|\boldsymbol{q}|^2} T_L(q) + \frac{q_0^2}{(q^2+i\epsilon)^2} T_T(q) \right) \tag{3.58}$$

with

$$T_L = T_{00}(q) = \int d\omega \; S_L(\omega, \boldsymbol{q}) \left(\frac{1}{q_0 - \omega + i\epsilon} - \frac{1}{q_0 + \omega - i\epsilon} \right), \tag{3.59}$$

and

$$T_T = \left(\delta_{ij} - \frac{q_i q_j}{|\boldsymbol{q}|^2} \right) T^{ij}(q) =$$
$$\text{Seagull} + \int d\omega \; S_T(\omega, \boldsymbol{q}) \left(\frac{1}{q_0 - \omega + i\epsilon} - \frac{1}{q_0 + \omega - i\epsilon} \right). \tag{3.60}$$

The transverse and longitudinal response functions are defined by:

$$S_L(\omega, \boldsymbol{q}) = \sum_{N \neq N_0} |\langle N||\hat{\rho}(\boldsymbol{q})||N_0\rangle|^2 \delta(\omega - \omega_N), \tag{3.61}$$

$$S_T(\omega, \boldsymbol{q}) = \sum_{\lambda=\pm1} \sum_{N \neq N_0} |\langle N||\hat{e}_\lambda^\dagger \cdot \boldsymbol{J}(\boldsymbol{q})||N_0\rangle|^2 \delta(\omega - \omega_N). \tag{3.62}$$

where $\rho(\boldsymbol{q})$, $\boldsymbol{J}(\boldsymbol{q})$ are the nuclear density and current. The transverse photon polarizations are $\lambda = \pm 1$. Carrying out the integration over q_0 we obtain:

$$\delta_{rel} = -8\alpha^2\phi^2(0)\int_0^\infty dq\,[R_L + R_T + R_S]\,F^2(\boldsymbol{q}^2), \tag{3.63}$$

$$\delta_{rel} = \delta_L^{(0)} + \delta_T^{(0)}, \tag{3.64}$$

where

$$\delta_L^{(0)} = -8\alpha^2\phi^2(0)\int_0^\infty dq\ R_L F^2(\boldsymbol{q}^2), \tag{3.65}$$

$$\delta_T^{(0)} = -8\alpha^2\phi^2(0)\int_0^\infty dq\,(R_T + R_S)\,F^2(\boldsymbol{q}^2). \tag{3.66}$$

Here, we have that $F(\boldsymbol{q}^2)$ is the nucleon form factor and R_L, R_T, R_S are the longitudinal, transverse and seagull kernel functions

$$R_L = \int_{\omega_{th}}^\infty d\omega\ S_L(\omega,\boldsymbol{q})g(\omega,\boldsymbol{q}), \tag{3.67}$$

$$R_T = \int_{\omega_{th}}^\infty d\omega\ S_T(\omega,\boldsymbol{q})\left[-\frac{1}{4m_r q}\frac{\omega+2q}{(\omega+q)^2} + \frac{q^2}{4m_r^2}g(\omega,q)\right], \tag{3.68}$$

$$R_S = \int_{\omega_{th}}^\infty d\omega\ S_T(\omega,0)\frac{1}{4m_r\omega}\left[\frac{1}{q} - \frac{1}{E_q}\right], \tag{3.69}$$

with

$$E_q = \sqrt{q^2 + m_r}, \tag{3.70}$$

$$g(\omega,q) = \frac{1}{2E_q}\left[\frac{1}{(E_q - m_r)(E_q - m_r + \omega)} - \frac{1}{(E_q + m_r)(E_q + m_r + \omega)}\right]. \tag{3.71}$$

It is convenient to calculate the response function by choosing the momentum transfer $\boldsymbol{q}$ to be along the $\hat{z}$ direction. However, this calculation is valid for any chosen

direction. The leading order longitudinal response function in the low momentum limit is given by:

$$S_L^{(0)}(\omega, \boldsymbol{q}) = \frac{4\pi}{9}(Z^2 q^2) S_{D1}(\omega). \tag{3.72}$$

The transverse response function can be broken up into the electric $S_T^{el}(\omega)$ and magnetic $S_T^{mag}(\omega)$ response functions as shown in Ref. [50]. Using the Siegert theorem, $\boldsymbol{q} \cdot \boldsymbol{J}(\boldsymbol{q}) = \omega\rho(\boldsymbol{q})$, the dominant transverse response function can be related to the electric dipole operator. At leading order, we obtain:

$$S_T^{(0)}(\omega, \boldsymbol{q}) = S_T^{el(0)}(\omega) + S_T^{mag(0)}(\omega), \tag{3.73}$$

$$S_T^{el(0)}(\omega) = \frac{8\pi}{9}(Z^2\omega^2) S_{D_1}(\omega), \tag{3.74}$$

$$S_T^{mag(0)}(\omega) = \frac{q^2}{6m_p^2}\left(\frac{g_p - g_n}{2}\right) S_{O_{ST}}(\omega), \tag{3.75}$$

$$\hat{O}_{ST} = \sum_i^A \boldsymbol{s}_i \tau_i^3. \tag{3.76}$$

Where m_p is the mass of the proton and g_p, g_n are the g-factors of the proton and neutron, respectively. Using the electric response function in equation (3.74), the integrals in equations (3.65) and (3.66) can be carried out. For the longitudinal and transverse corrections, after subtracting out the leading non-relativistic expression, we obtain our relativistic longitudinal $\delta_L^{(0)}$, and transverse $\delta_T^{(0)}$ energy corrections,

$$\delta_L^{(0)} = \frac{16\pi}{9}(Z\alpha)^2\phi^2(0)\int_{\omega_{th}}^{\infty} d\omega \ \left(2\mathcal{G}\left(\frac{\omega}{m_r}\right) + \pi\sqrt{\frac{2m_r}{\omega}}\right) S_{D1}(\omega), \tag{3.77}$$

$$\delta_T^{(0)} = \frac{16\pi}{9}(Z\alpha)^2\phi^2(0)\int_{\omega_{th}}^{\infty} d\omega \ \left(\frac{\omega}{m_r} + \frac{\omega}{m_r}\ln\left(\frac{2\omega}{m_r}\right) + \frac{\omega^2}{m_r^2}\mathcal{G}\left(\frac{\omega}{m_r}\right)\right) S_{D1}(\omega). \tag{3.78}$$

Where $S_{\hat{D}_1}(\omega)$ is the dipole response function defined in equation (3.36), and $\mathcal{G}(x)$ is

defined as

$$\mathcal{G}(x) = \sqrt{\frac{x-2}{x}}\text{Arctanh}\left(\sqrt{\frac{x-2}{x}}\right) - \sqrt{\frac{x+2}{x}}\text{Arctanh}\left(\sqrt{\frac{x}{x+2}}\right). \tag{3.79}$$

To obtain the magnetic polarizability term, we take the magnetic response function defined in equation (3.76) and carry out the integral in equation (3.66). Because the magnetic polarizability term is quite small, we can take the leading order term in the integral. The result of this approximation gives us the magnetic polarizability correction $\delta_M^{(0)}$:

$$\delta_M^{(0)} = \frac{8\pi}{3}\alpha^2\phi^2(0)\left(\frac{g_p - g_n}{4m_p}\right)^2 \int_{\omega_{th}}^{\infty} d\omega \, \sqrt{\frac{\omega}{2m_r}} S_{O_{ST}}(\omega). \tag{3.80}$$

3.3 Finite Nucleon Size Effects

Finally, we consider the finite size of the nucleons, which in our previous considerations were treated as point like. To take account of these corrections we introduce the correction ΔH as

$$\Delta H = \sum_{a=1}^{A} \Delta V_a(\boldsymbol{r}, \boldsymbol{R}_a), \tag{3.81}$$

$$\Delta V_a(\boldsymbol{r}, \boldsymbol{R}_a) = \alpha\left(\frac{\hat{e}_{p,a}}{r} - \int d\boldsymbol{R}\frac{n_a(\boldsymbol{R}' - \boldsymbol{R}_a)}{|\boldsymbol{r} - \boldsymbol{R}|}\right). \tag{3.82}$$

Here, we have that the nucleon charge density $n_a(\boldsymbol{R})$, is the sum of the neutron an proton charge densities.

$$n_a(\boldsymbol{R}) = \hat{e}_{n,a} n_n(\boldsymbol{R}) + \hat{e}_{p,a} n_p(\boldsymbol{R}), \tag{3.83}$$

where the proton and neutron charge densities, $n_p(\boldsymbol{x})$ and $n_n(\boldsymbol{x})$ respectively, satisfy:

$$1 = \int n_p(\boldsymbol{x}) d\boldsymbol{x}, \tag{3.84}$$

$$0 = \int n_n(\boldsymbol{x}) d\boldsymbol{x}, \tag{3.85}$$

and

$$\langle r_p^2 \rangle = \int \boldsymbol{x}^2 n_p(\boldsymbol{x}) d\boldsymbol{x}, \tag{3.86}$$

$$\langle r_n^2 \rangle = \int \boldsymbol{x}^2 n_n(\boldsymbol{x}) d\boldsymbol{x}, \tag{3.87}$$

with the proton and neutron projection isospin operators are given by

$$\hat{e}_{n,a} = \frac{1 - \tau_{z,a}}{2}, \tag{3.88}$$

$$\hat{e}_{p,a} = \frac{1 + \tau_{z,a}}{2}. \tag{3.89}$$

With these operators, the energy correction due to the finite nuclear size is given by

$$\delta_{NR} = - \sum_{c,c'=n,p} \sum_{N \neq N_0} \int d\boldsymbol{R} \int d\boldsymbol{R}' \rho_N^{c*}(\boldsymbol{R}) P_{NR}^{cc'}(\boldsymbol{R}, \boldsymbol{R}', \omega_N) \rho_N^{c}(\boldsymbol{R}'), \tag{3.90}$$

like in the earlier non-relativistic treatment. Each of the above correlation functions can be evaluated in momentum space as

$$P_{NR}^{pp}(\boldsymbol{R}, \boldsymbol{R}', \omega_N) = -16 m_r \alpha^2 Z^2 \phi^2(0) \int_0^\infty dq \, \frac{\left(\tilde{n}_p^2(q) \frac{\sin(q|\boldsymbol{R}-\boldsymbol{R}'|)}{q|\boldsymbol{R}-\boldsymbol{R}'|} - 1 \right)}{q^2 \left(q^2 + 2 m_r \omega_N \right)}, \tag{3.91}$$

$$P_{NR}^{pn}(\boldsymbol{R}, \boldsymbol{R}', \omega_N) = -16 m_r \alpha^2 N Z \phi^2(0) \int_0^\infty dq \, \frac{\left(\tilde{n}_n(q) \tilde{n}_p(q) \frac{\sin(q|\boldsymbol{R}-\boldsymbol{R}'|)}{q|\boldsymbol{R}-\boldsymbol{R}'|} \right)}{q^2 \left(q^2 + 2 m_r \omega_N \right)}, \tag{3.92}$$

$$P_{NR}^{nn}(\boldsymbol{R}, \boldsymbol{R}', \omega_N) = -16 m_r \alpha^2 N^2 \phi^2(0) \int_0^\infty dq \, \frac{\left(\tilde{n}_n^2(q) \frac{\sin(q|\boldsymbol{R}-\boldsymbol{R}'|)}{q|\boldsymbol{R}-\boldsymbol{R}'|} \right)}{q^2 \left(q^2 + 2 m_r \omega_N \right)}, \tag{3.93}$$

where we have introduced the Fourier transform of the proton an neutron charge distributions, $\tilde{n}_p(q)$ and $\tilde{n}_n(q)$, respectively. In order to calculate these integrals, we will require knowledge of the neutron and proton form factors. A phenomenological model of these form factors is given by a dipole fit of scattering experiments, known as Sachs form factors as [51]:

$$\tilde{n}_n(q) = \frac{\lambda q^2}{(1+\frac{q^2}{\beta^2})^3} \approx \lambda q^2 \tag{3.94}$$

$$\tilde{n}_p(q) = \frac{1}{(1+\frac{q^2}{\beta^2})^2} \approx 1 - \frac{2q^2}{\beta^2} \tag{3.95}$$

with $\beta = 4.120$ fm^{-1}, and $\lambda = 0.01935$ fm^2. We consider the products of the form factors in equations (3.91),(3.92) and (3.93) only up to quadratic terms in q. For the proton-proton correlation, we have:

$$P_{NR}^{pp} \approx \frac{2\pi\alpha^2 Z^2}{3}\phi^2(0)\frac{2m_r}{\omega_N}\left(|\boldsymbol{R}-\boldsymbol{R}'|^2 - \frac{1}{4}\sqrt{2m_r\omega_N}|\boldsymbol{R}-\boldsymbol{R}'|^3 + \frac{1}{10}|\boldsymbol{R}-\boldsymbol{R}'| + ...\right)$$
$$+ \frac{2\pi\alpha^2 Z^2}{3}\phi^2(0)\sqrt{\frac{2m_r}{\omega_N}}\frac{4}{\beta^2}\left(6 - 3\sqrt{2m_r\omega_N}|\boldsymbol{R}-\boldsymbol{R}'| + 2m_r\omega_N|\boldsymbol{R}-\boldsymbol{R}'|^2 + ...\right). \tag{3.96}$$

The leading order nucleon size corrections are then obtained from this expression by subtracting out the point nucleus contribution and discarding terms independent of $\boldsymbol{R}$ or $\boldsymbol{R}'$, which do not contribute to the energy due to the orthogonality of the nuclear states. The weight independent term in this expression will give us the inelastic contribution $\delta_{NR}^{(pp-R1)}$ to the Lamb shift. This correction is given by,

$$\delta_{NR}^{(pp-R1)} = -4\pi\alpha^2 Z^2 m_r \phi^2(0)\frac{4}{\beta^2}\int d\boldsymbol{R}\int d\boldsymbol{R}'|\boldsymbol{R}-\boldsymbol{R}'|\left(\rho_0^{pp}(\boldsymbol{R},\boldsymbol{R}') - \rho_0^p(\boldsymbol{R})\rho_0^p(\boldsymbol{R}')\right), \tag{3.97}$$

where the proton-proton 2-body density is given by,

$$\rho_0^{pp}(\boldsymbol{R},\boldsymbol{R}') = \langle N_0|\frac{1}{Z^2}\sum_{a,b}\delta(\boldsymbol{R}-\boldsymbol{R}_a)\delta(\boldsymbol{R}'-\boldsymbol{R}_b)\hat{e}_{p,a}\hat{e}_{p,b}|N_0\rangle. \tag{3.98}$$

For the deuteron, the proton-proton 2-body density vanishes, so we obtain,

$$\delta_{NR}^{(pp-R1)} = 4\pi\alpha^2 Z^2 m_r \phi^2(0) \frac{4}{\beta^2} \langle r \rangle_{(2)}. \tag{3.99}$$

The $|\boldsymbol{R}-\boldsymbol{R}'|^2$ in equation (3.96) can then be evaluated in terms of spherical harmonics. This will give us the leading order inelastic, finite size correction $\delta_{NR}^{(pp-R2)}$ as,

$$\delta_{NR}^{(pp-R2)} = -\frac{16m_r^2}{\beta^2}\frac{16\pi^2}{9} Z^2\alpha^2\phi^2(0) \int\limits_{\omega_{th}}^{\infty} d\omega \, \sqrt{\frac{\omega}{2m_r}} S_{D1}(\omega). \tag{3.100}$$

Similarly, we find that the neutron-proton overlap integral gives us,

$$\begin{aligned} P_{NR}^{np-overlap} &= P_{NR}^{np} + P_{NR}^{pn} = 2P_{NR}^{np} \\ &\approx \frac{2\pi\alpha^2 Z^2}{3}\phi^2(0)\sqrt{\frac{2m_r}{\omega_N}}(-2\lambda)\left(6 - 3\sqrt{2m_r\omega_N}|\boldsymbol{R}-\boldsymbol{R}'| + 2m_r\omega_N|\boldsymbol{R}-\boldsymbol{R}'|^2 + ...\right), \end{aligned} \tag{3.101}$$

the energy independent leading order term, gives us the inelastic $\delta_{NR}^{(np-R1)}$ term,

$$\delta_{NR}^{(np-R1)} = 8\pi\lambda\alpha^2 Z^2 m_r \phi^2(0) \int d\boldsymbol{R} \int d\boldsymbol{R}' |\boldsymbol{R}-\boldsymbol{R}'| \left(\rho_0^{pn}(\boldsymbol{R},\boldsymbol{R}') - \rho_0^n(\boldsymbol{R})\rho_0^p(\boldsymbol{R}')\right). \tag{3.102}$$

The term in equation (3.101) depending on $|\boldsymbol{R}-\boldsymbol{R}'|^2$ will give us a finite size correction $\delta_{NR}^{(np-R2)}$ that depends on the dipole response function,

$$\delta_{NR}^{(np-R2)} = -8\lambda m_r^2 \frac{16\pi^2}{9}(Z\alpha)^2\phi^2(0) \int_{\omega_{th}}^{\infty} d\omega \, \sqrt{\frac{\omega}{2m_r}} S_{D1}(\omega). \tag{3.103}$$

The finite nucleon size corrections that we calculate are then written as,

$$\delta_{NS}^{(1)} = \delta_{NR}^{pp-R1} + \delta_{NR}^{np-R1}, \tag{3.104}$$

$$\delta_{NS}^{(2)} = \delta_{NR}^{pp-R2} + \delta_{NR}^{np-R2}, \tag{3.105}$$

where $\delta_{NS}^{(1)}$ constitute the leading nucleon size-corrections and $\delta_{NS}^{(2)}$ are the sub-leading corrections. In addition, the momentum expansion of nucleon form factors does not produce corrections that depend on the proton and neutron Zemach moments which must be included as was done in by Ref. [30]. For a nucleus of mass number A this correction amounts to,

$$-\frac{\pi\alpha^2}{3}m_r\phi^2(0)\left(Z\langle r_p^3\rangle_{(2)}+N\langle r_n^3\rangle_{(2)}\right). \tag{3.106}$$

3.4 Alternate P_{NR} Expansion

In Section 3.2, we obtained the nuclear polarizability corrections by performing the integral over the momentum and then expanding the resulting expression in terms of nuclear excitation operators. This method is very useful for obtaining analytical results to a given order, however, extending this method for higher orders is difficult, therefore, we consider an alternative way of calculating P_{NR} which automatically includes corrections to all orders. The idea is to use the partial wave decomposition of the complex exponential in equation (3.25),

$$e^{i\boldsymbol{q}\cdot\boldsymbol{s}}=4\pi\sum_{\ell,m}i^\ell j_\ell(qs)Y_m^\ell(\hat{s})Y_m^\ell(\hat{q})^*. \tag{3.107}$$

Similarly, we expand $e^{-i\boldsymbol{q}\cdot\boldsymbol{s}'}$ and integrate over the angles $\hat{q}$,

$$P_{NR}(\boldsymbol{s},\boldsymbol{s}')=\frac{16}{\pi}(\alpha Z)^2\sum_{\ell=0}^{\infty}\int_0^\infty dq\ \frac{(j_\ell(qs')-\delta_{\ell,0})(j_\ell(qs)-\delta_{\ell,0})Y_m^\ell(\hat{s})Y_m^\ell(\hat{s}')^*}{q^2(\frac{q^2}{2m_r}+\omega_N)}. \tag{3.108}$$

Re-inserting the completeness of nuclear states into this expression we have,

$$P_{NR}=\frac{16}{\pi}(\alpha Z)^2\sum_{\ell=0}^{\infty}\int_0^\infty dqR_\ell(q), \tag{3.109}$$

where we have introduced the response function for a particular multipole ℓ to be given by,

$$R_\ell(q) = \frac{1}{q^2}\int\limits_{\omega_{th}}^{\infty} d\omega \frac{S_\ell(\omega,q)}{q^2(\frac{q^2}{2m_r}+\omega_N)} \tag{3.110}$$

$$S_\ell(\omega,q) = \frac{1}{2J_0+1}\frac{1}{Z}\sum_f |\langle f||(j_\ell(qs)-\delta_{\ell,0})Y^\ell(\hat{s})||i\rangle|^2\delta(E_f-E_i-\omega). \tag{3.111}$$

This alternative expansion has the advantage that all of the nuclear polarizability corrections corresponding to a particular multipole are contained in the response function $R_\ell(q)$. Some results obtained using this formalism will be presented in Chapter 4.

Chapter 4

Results

In this chapter the results of numerical benchmarks and the nuclear structure corrections in μD for different nuclear potentials are presented. The convergence of these results in orders of chiral effective field theory is analysed to produce an estimate of the theoretical uncertainty.

Nuclear polarizability corrections are basically calculated by integrating the product of the response function $S_{\hat{O}}(\omega)$ of an operator $\hat{O}$ with a weight function $g(\omega)$,

$$\delta_{\hat{O}} = \int_{\omega_{th}}^{\infty} g(\omega) S_{\hat{O}}(\omega) d\omega, \tag{4.1}$$

where,

$$S_{\hat{O}}(\omega) = \frac{1}{2J_0+1} \sum_{N \neq N_0} |\langle N||\hat{O}||N_0\rangle|^2 \delta\left(E_N - E_0 - \omega\right). \tag{4.2}$$

The deuteron response functions are calculated by expanding the states $|N_0\rangle$ and $|N\rangle$ in a truncated harmonic oscillator basis (HO). The general form of this expansion for

a state $|N\rangle$ is,

$$|N\rangle = \sum_{i}^{\mathrm{N}_{Max}} c_i |n, (lS)J, T; M_l, M_T\rangle, \tag{4.3}$$

where n is the principal quantum number, l the relative orbital angular momentum, S the spin of the nucleus, J the total angular momentum, T the total isospin, and M_l, M_T are the projections of l and T respectively. The integer i is the collective index of the allowable quantum numbers. The parameter N_{Max} parametrizes the dimensions of the model space and determines the allowed values of the principle quantum number n and angular momentum l through the harmonic oscillator condition $\mathrm{N}_{Max} \leq 2n + l$. This expansion is only exact in the limit where the model space size is infinite, therefore truncation requires that our calculations are checked for convergence in N_{Max}. The coefficients c_i are the components of the eigenvectors corresponding to the discretized nuclear Hamiltonian. The model space size for the deuteron remained tractable, allowing the nuclear Hamiltonian to be diagonalized with LAPACK routines implemented in Fortran.

In the coordinate representation, the HO-basis functions are given by,

$$\langle \boldsymbol{r}|n, l; m\rangle = N(n, l) L_n^{l+\frac{1}{2}}(2\nu r^2) e^{-\nu r^2} r^l Y_m^l(\hat{r}), \tag{4.4}$$

$$N(n, l) = \sqrt{\frac{(2n)!(2\nu)^{l+\frac{3}{2}}}{\Gamma(n + l + \frac{3}{2})}}, \tag{4.5}$$

$$\nu = \frac{M_r \Omega}{2\hbar}, \tag{4.6}$$

where M_r is the reduced mass of the proton and neutron system and Ω is the harmonic oscillator frequency.

The matrix elements of the Hamiltonian consist of the kinetic, $\langle a|\hat{T}|c\rangle$ term, and

the two-body nuclear matrix elements $\langle a|\hat{V}_{NN}|c\rangle$ determined with the desired NN-force, where $|a\rangle = |n_a, (l_a S_a) J_a, T_a; \rangle$ and $|c\rangle = |n_c, (l_c S_c) J_c, T_c; \rangle$.

In this work, we have used the AV18 potential [36] and nuclear potentials derived from chiral effective field theory as outlined by Epelbaum *et al.* [52, 40]. The χ_{EFT} potentials developed by Epelbaum *et al.* are a set of chiral potentials truncated at different orders and with varying cut offs. The pairs of cut offs used, $\{\Lambda, \tilde{\Lambda}\}$ where Λ is the Lippmann-Schwinger cut off and $\tilde{\Lambda}$ is the SFR cut off are shown in Table 4.1.

	NLO	N^2LO	N^3LO
$\{\Lambda, \tilde{\Lambda}\}$ [MeV]	$\{400, 700\}$	$\{450, 700\}$	$\{450, 700\}$
	$\{550, 700\}$	$\{550, 600\}$	$\{550, 700\}$
		$\{600, 700\}$	$\{600, 700\}$

Table 4.1: The cut off combinations for different chiral orders used in the Epelbaum *et al.* potentials [52].

The Epelbaum *et al.* potentials will be referred to individually as $N^kLO(\Lambda,\tilde{\Lambda})$ and collectively as N^kLO-EGM. We also use the χ_{EFT} nuclear potential developed by Entem and Machleidt [40] which is a N^3LO potential with a fixed $\Lambda = 500$ MeV cut off and will be referred to as N^3LO-EM. The matrix elements of the AV18 and the N^3LO-EM potentials in the HO-basis are generated by a code written by Nir Barnea, while the code for the N^kLO-EGM matrix elements in the HO-basis was provided by Epelbaum [53].

4.1 Numerical Checks

Numerical benchmarks were performed by comparing our calculations of deuteron ground state expectation values using the AV18 and χ_{EFT} to results obtained by Refs. [36, 40, 52]. The computed ground state properties were the binding energy E_0, the structure radius $\langle r_{str}^2 \rangle_d^{1/2}$, the quadrupole moment Q_d, and the D-wave probability P_D defined in Chapter 2. The results of these calculations are listed in Table 4.2. Explored in Figure 4.1 and 4.2 is the convergence of the deuteron ground state properties as a function of the model space size N_{Max} for different values of the harmonic oscillator parameter $\hbar\Omega$ in MeV.

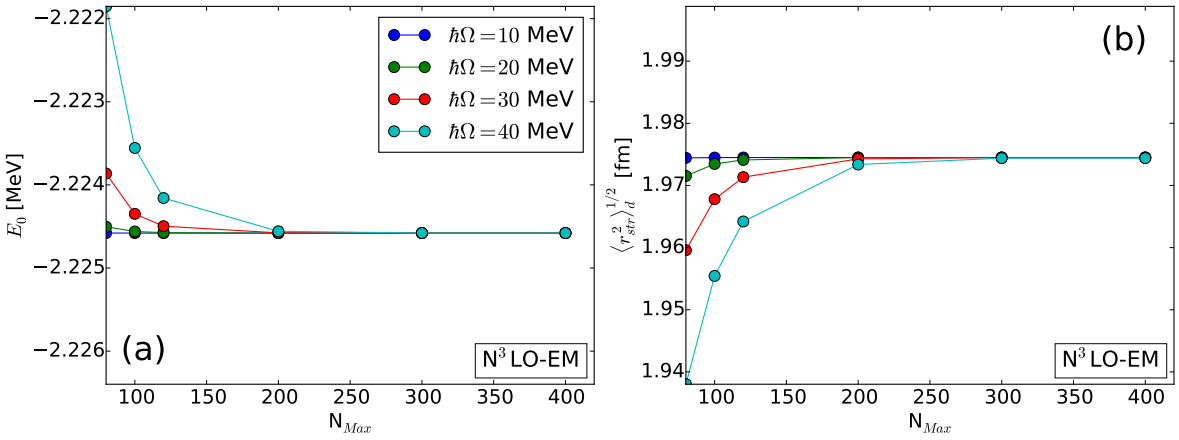

Figure 4.1: Convergence of (a) the deuteron binding energy E_0 and (b) the structure radius $\langle r_{str}^2 \rangle_d^{1/2}$ as a function of N_{Max} parametrizing the size of the model space for the N^{3}LO-EM potential.

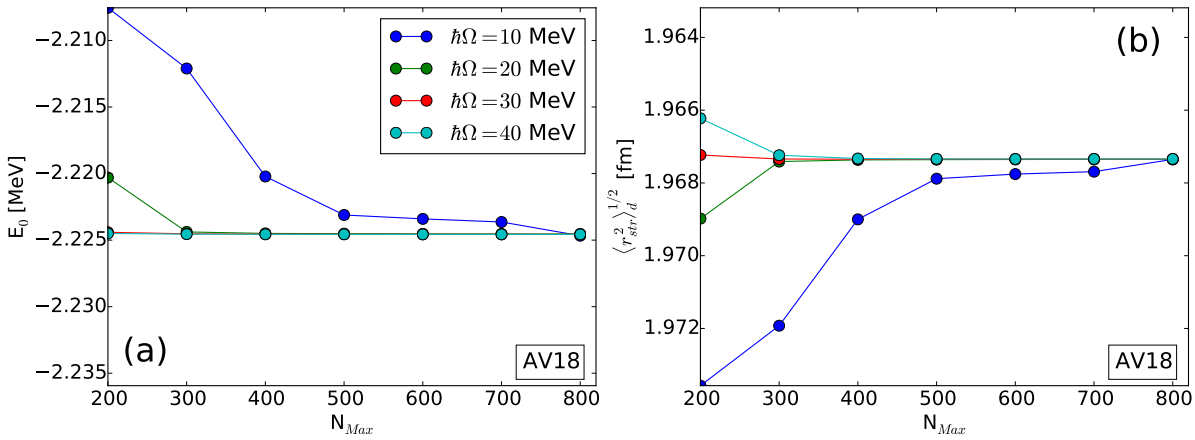

Figure 4.2: Convergence of (a) the deuteron binding energy E_0 and (b) the structure radius $\langle r_{str}^2 \rangle_d^{1/2}$ as a function of N_{Max} parametrizing the size of the model space for the AV18 potential.

These figures illustrate the convergence of the deuteron ground state properties towards the exact values which are stable with respect to variations of $\hbar\Omega$. This is expected since the $\hbar\Omega$ dependence of our calculations is an artefact of a limited basis size. We observe that there exist optimal values of $\hbar\Omega$ that accelerate the convergence of the deuteron properties. For example, $\hbar\Omega$ =30 MeV leads to a quick convergence for all observables. By contrast, we see that $\hbar\Omega$ =10 MeV produces the slowest convergence of the deuteron ground state properties. We also observe that the N^{3}LO-EM potential requires a smaller model space with respect to AV18 potential to exhibit convergence. This is because the AV18 potential has stronger repulsion at short distances which requires a larger kinetic energy to penetrate into the potentials at short distances. Converged results are listed in Table 4.2 for the AV18, N^{3}LO-EM and N^{3}LO-EGM potentials. The range in the N^{3}LO-EGM columns is obtained by varying the cut offs as in Table 4.1.

	AV18	N^{3}LO-EM	N^{3}LO-EGM
E_0 [MeV]	2.2246	2.2246	(2.2189, 2.2235)
$\langle r^2_{str}\rangle^{1/2}_d$ [fm]	1.967	1.974	(1.975, 1.979)
Q_d [fm^2]	0.2697	0.2750	(0.2659, 0.2692)
P_D [%]	5.760	4.514	(2.844, 3.634)

Table 4.2: The converged results of the deuteron ground state observables.

In Table 4.3 we compare our results to the published literature that used the AV18 potential and observe very good agreement showing the reliability of our numerical methods.

		E_0 [MeV]	$\langle r^2_{str}\rangle^{1/2}_d$ [fm]	Q$_d$ [fm^2]	P_D [%]
N^{3}LO-EM	This work	2.2246	1.974	0.275	4.51
	This work +RC+MEC	–	1.978	0.285[1]	–
	Ref. [40]	2.2246	1.978	0.285[1]	4.51
AV18	This work	2.2246	1.967	0.270	5.76
	Ref. [36]	2.2246	1.967	0.270	5.76
Experiment		2.224573(2)[1]	1.97507(78)[2]	0.285783(30)[3]	–

[1]Ref. [21],[2]Ref. [24], [3]Ref. [22]

Table 4.3: Comparison of our deuteron calculations to results by Entem and Machleidt [40] and Wiringa *et al.* [36].

To compare our calculated values of Q_d and $\langle r^2_{str}\rangle^{1/2}_d$ to the work of Ref. [40], we added to our calculations phenomenological relativistic corrections and meson exchange current corrections to both the charge (0.0145 fm^2) and quadrupole operator (0.01 fm^2). Meson exchange currents (MEC) arise as higher order contributions to the electromagnetic currents in nuclei from the interaction of photons with the exchanged charged pions. These electromagnetic currents are intimately linked to the nuclear

potential through the requirement of charge conservation. An example of two-body MECs is shown in Figure 4.3.

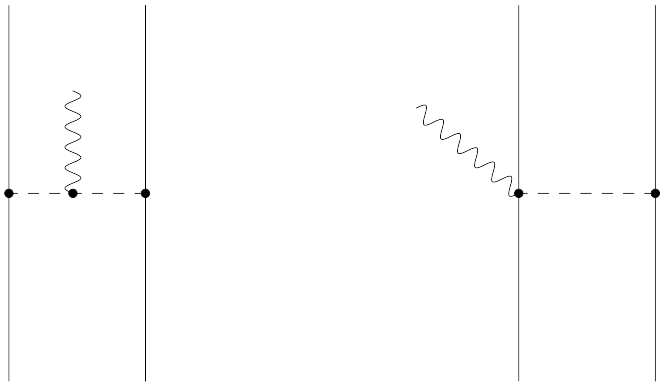

Figure 4.3: Pion exchange current diagrams [54]; Pion in flight (left) and contact term (right). Nucleons are represented by solid lines, dashed lines are for the pions, and the curved line is the photon.

The effects of MEC on the electromagnetic properties of nuclei has been widely studied and it has been found that the inclusion of MEC may be required to achieve agreement with experiment. In Table 4.3 we observe that the addition of phenomenological MEC contributions allow the quadrupole moment and structure radius to be consistent with the most recent experimental results.

In Fig. 4.4, the results of E_0, Q_d and $\langle r^2_{str}\rangle^{1/2}_d$ are shown from chiral potentials at different orders in χ_{EFT}. The bands are produced through cut off variations of the N^{k}LO-EGM potentials that serve as estimates of the theoretical uncertainties. For the binding energy, the size of the bands decreases with increasing chiral order and converge to the results of the N^{3}LO-EM and AV18 potentials that have been fitted to experiment. The values of Q_d produced by the χ_{EFT} potentials at N^{3}LO and the AV18 potential do not overlap with the experimental value due to missing MEC in

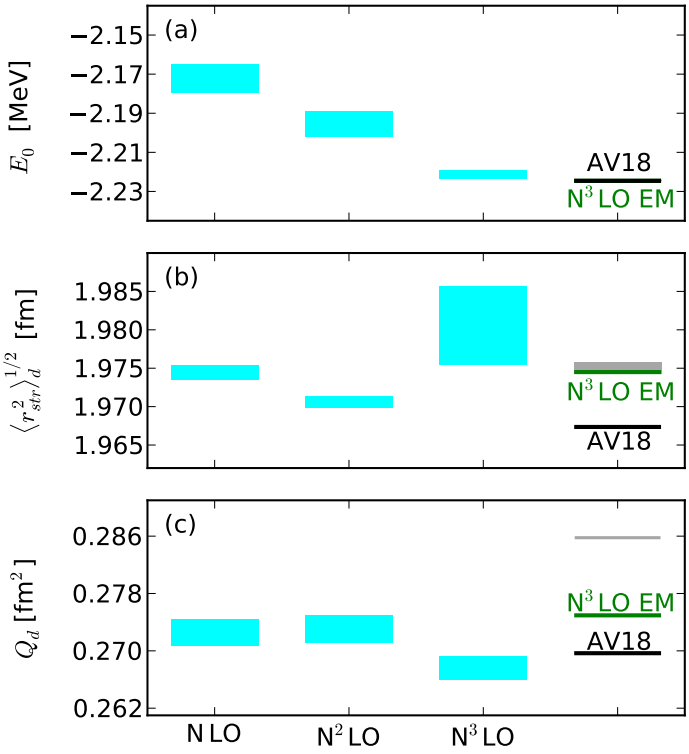

Figure 4.4: Deuteron ground state properties for different potential models: (a) binding energy, (b) structure radius, and (c) quadrupole moment. The blue bands are obtained from cut off variations of the N^{k}LO-EGM potentials. The grey bands are experimental values.

the calculations. The bands of the structure radius decrease from NLO to N^{2}LO, but then spread at N^{3}LO. This behaviour, noted also by Ref. [52], is attributed to the necessity of consistent MEC at the N^{3}LO level not included here and which would reduce the observed cut off dependence.

Having tested ground state observables, we proceed to test the numerics of observables that depend on the excited states of the deuteron. Two such observables that have been calculated by a number of groups are the electric and magnetic polarizabilities, α_E and β_M. These electromagnetic polarizabilities measure a system's linear response to an applied electromagnetic field. At leading order, an external electric

$\boldsymbol{E}$, or magnetic $\boldsymbol{B}$ field induces an electric $\boldsymbol{D}$ or magnetic $\boldsymbol{M}1$ dipole moment in the object proportional to the strength of the external source,

$$\boldsymbol{D} = \alpha_E \boldsymbol{E}, \tag{4.7}$$

$$\boldsymbol{M}1 = \beta_M \boldsymbol{B}. \tag{4.8}$$

The electromagnetic polarizabilities are then the constants of proportionality in these expressions. These expressions can be calculated as,

$$\alpha_E = \frac{2\alpha}{3} \sum_{N \neq N_0} \frac{|\langle N|\boldsymbol{D}|N_0\rangle|^2}{E_N - E_0}, \tag{4.9}$$

$$\beta_M = \frac{2\alpha}{3} \sum_{N \neq N_0} \frac{|\langle N|\boldsymbol{M}1|N_0\rangle|^2}{E_N - E_0}. \tag{4.10}$$

The results of these calculations for the AV18 and χ_{EFT} potentials at order N^{3}LO are presented in Table 4.4. Our results for α_E with the AV18 agree within 0.2% of Ref. [55] and β_M agrees within 0.1% of Ref. [56] which used the same potential.

	AV18 (Friar)	AV18	N^{3}LO-EM	N^{3}LO-EGM
α_E [fm^3]	0.634[1]	0.633	0.633	(0.633, 0.637)
β_M [fm^3]	0.0679[2]	0.0678	0.0684	(0.0689, 0.0695)

[1]Ref. [55],[2]Ref. [56]

Table 4.4: Results of the electric and magnetic polarizabilities with different potentials.

4.2 Nuclear Structure Corrections

Before proceeding to our results with the χ_{EFT} potentials, it is necessary to compare our calculations of the nuclear structure corrections for the AV18 potential with previous work. Pachucki was the first to calculate these nuclear structure corrections for μD in Ref. [20]. However, following the publication of our work in Ref. [57], Pachucki then improved his calculations and added an additional relativistic term δ_{HO} to the Lamb shift Ref. [58]. The comparison of our calculations with the AV18 potential to that of Pachucki is shown in Table 4.5.

		Pachucki 2011 [20]	Our Work	Pachucki 2015 [58]
$\delta^{(0)}$	$\delta^{(0)}_{D1}$	-1.910	-1.907	-1.910
	$\delta^{(0)}_{L}$	0.035	0.029	0.026
	$\delta^{(0)}_{T}$	–	-0.012	–
	δ_{HO}	–	–	-0.004
	$\delta^{(0)}_{C}$	0.261	0.262	0.261
	$\delta^{(0)}_{M}$	0.016	0.008	0.008
$\delta^{(1)}$	$\delta^{(1)}_{Z3}$	–	0.357	–
$\delta^{(2)}$	$\delta^{(2)}_{R2}$	0.045	0.042	0.042
	$\delta^{(2)}_{Q}$	0.066	0.061	0.061
	$\delta^{(2)}_{D1D3}$	-0.151	-0.139	-0.139
δ_{NS}	$\delta^{(1)}_{Z1}$	–	0.064	–
	$\delta^{(1)}_{np}$	–	0.017	0.018
	$\delta^{(2)}_{NS}$	–	-0.020	-0.020
$\delta^{A}_{\rm pol}$		–	-1.240	–
$\delta_{\rm Zem}$		–	-0.421	–
$\delta^{A}_{\rm pol} + \delta_{\rm Zem}$		-1.638	-1.661	-1.657

Table 4.5: Comparison of nuclear polarization contributions to the $2S$-$2P$ Lamb shift ΔE [meV] in μD using the AV18 potential.

We found very good agreement with the leading order dipole correction. The small 0.2% difference between our results is due to the fact that Pachucki takes into account the small mass difference between the proton and neutron. There are small, but non-negligible differences that appear in the relativistic corrections due to the fact that Pachucki [20] has Taylor expanded the relativistic integral in Section 3.2.2 to leading order, whereas we have used the full expression. We also observed an $\approx 8\%$ difference in the $\delta^{(2)}_{R2}$, $\delta^{(2)}_{Q}$, $\delta^{(2)}_{D1D3}$ terms due to Pachucki having used the muon mass in his formulas, whereas we have used the reduced mass. Pachucki has since adopted our convention in Ref. [58] and now agrees with us. The Coulomb correction $\delta^{(0)}_{C}$ agrees with Pachucki within 0.4%. The small difference is due to the use of different formulas for calculating this correction. Our value of the magnetic dipole contribution is $\delta^{(0)}_{M}$ is 50% smaller than what was obtained by Pachucki [20], despite the fact that the same formula was used. The calculation of β_M which was in line with previously published results served as a useful check of our numerics. In addition, we calculated $\delta^{(0)}_{M}$ using the M1 response function from Arenhövel [26, 59] and obtained $\delta^{(0)}_{M} = 0.0067$ meV, in agreement with our value. In his most recent publication Pachucki found that this discrepancy was due to an error in his code and has subsequently corrected his value [58] so that our results agree. We also found a wrong sign in our derivation for $\delta^{(2)}_{NS}$ and corrected the final number from -0.015 meV to -0.020 meV.

The full compilation of our results for the nuclear structure corrections are listed in Table 4.6. The range listed in the N^{3}LO-EGM column is obtained by varying the cut off. These results can be used to estimate the nuclear physics error.

		AV18	N^{3}LO-EM	N^{3}LO-EGM
$\delta^{(0)}$	$\delta^{(0)}_{D1}$	-1.907	-1.912	(-1.911,-1.926)
	$\delta^{(0)}_{L}$	0.029	0.029	(0.029, 0.030)
	$\delta^{(0)}_{T}$	-0.012	-0.012	-0.013
	$\delta^{(0)}_{C}$	0.262	0.262	(0.262, 0.264)
	$\delta^{(0)}_{M}$	0.008	0.007	0.007
$\delta^{(1)}$	$\delta^{(1)}_{Z3}$	0.357	0.359	(0.359, 0.363)
$\delta^{(2)}$	$\delta^{(2)}_{R2}$	0.042	0.041	0.041
	$\delta^{(2)}_{Q}$	0.061	0.061	0.061
	$\delta^{(2)}_{D1D3}$	-0.139	-0.139	(-0.139,-0.140)
δ_{NS}	$\delta^{(1)}_{Z1}$	0.064	0.064	(0.064, 0.065)
	$\delta^{(1)}_{np}$	0.017	0.017	0.017
	$\delta^{(2)}_{NS}$	-0.020	-0.021	-0.021
$\delta^{A}_{\rm pol}$		-1.240	-1.243	(-1.242,-1.252)
$\delta_{\rm Zem}$		-0.421	-0.423	(-0.424,-0.428)
$\delta^{A}_{\rm pol}+\delta_{\rm Zem}$		-1.661	-1.667	(-1.666,-1.680)

Table 4.6: The results of nuclear polarization contributions to the $2S$-$2P$ Lamb shift in meV for μD with different potentials.

4.2.1 Total Error Budget

The average of all N^{3}LO and AV18 potential in Table 4.6 is $\delta^A_{pol} = -1.245$ meV with a 1σ uncertainty of 0.005 meV. Similarly, we find $\delta_{Zem} = -0.424 \pm 0.003(1\sigma)$.

In Figure 4.5 the convergence behaviour of $\delta^{(0)}_M$, $\delta^{(0)}_{D1}$, and $\delta^A_{pol} + \delta_{Zem}$ is plotted and the bands are obtained by varying the cut offs as before. The convergence of $\delta^A_{pol} + \delta_{Zem}$ is dominated by the largest correction $\delta^{(0)}_{D1}$. From N^{2}LO to N^{3}LO in the χ_{EFT} expansion, the value $\delta^A_{pol} + \delta_{Zem}$ changes by 0.3%. This spread is the systematic error due to truncating the potentials at this order and needs to be included in the total error budget. There is an additional estimated error of 1% from atomic physics

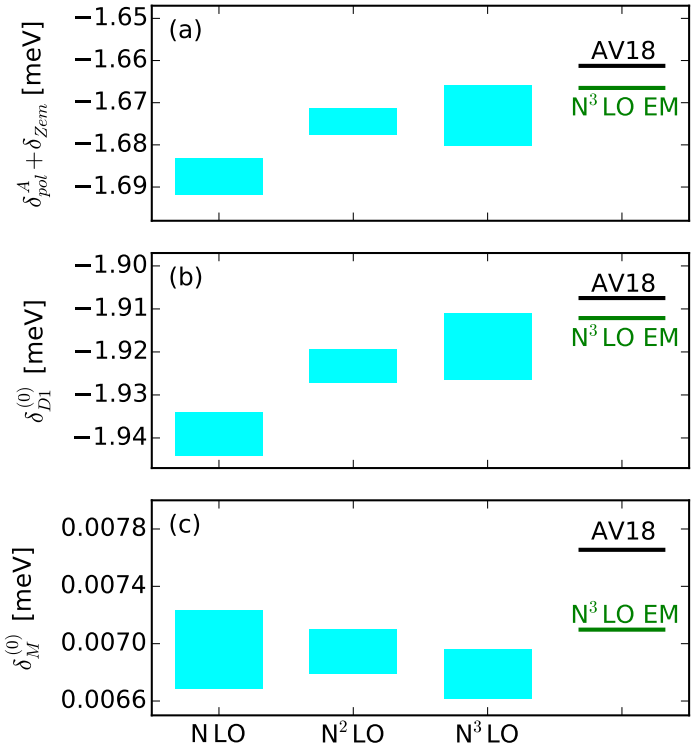

Figure 4.5: Total nuclear structure corrections (a), leading order dipole contribution (b) and the magnetic dipole correction (c) at different orders in χ_{EFT}. The blue bands are obtained from cut off variations of the N^{k}LO-EGM potentials.

[20]. This error is a result of neglecting correction terms that are of order $(Z\alpha)^6$ and higher.

	Error [%]
$\delta^A_{pol}+\delta_{Zem}$ (1σ)	0.5
Chiral convergence	0.3
Atomic physics	1
Total Error	1.16

Table 4.7: The total error budget of the nuclear structure corrections.

Adding the errors in Table 4.7 as a quadrature sum, the precision of the nuclear structure corrections is 1.16%. In total, we have that,

$$\delta^A_{pol} + \delta_{Zem} = -1.669 \pm 0.020 \text{ meV}. \tag{4.11}$$

For the nucleon polarizability corrections introduced after equation (1.1), we have adopted the best value of $\delta^N_{TPE} = -0.0470(0.0101)$ meV [17] that includes the nucleon polarizabilites δ^N_{pol} along with the nucleon Zemach corrections in equation (3.106). This gives us the total two-photon exchange corrections $\delta_{TPE} = \delta^A_{pol} + \delta^N_{TPE} + \delta_{Zem}$ value of

$$\delta_{TPE} = -1.716 \pm 0.022 \text{ meV}^1. \tag{4.12}$$

This is the number that the experimentalists [17] will use to extract r^2_{ch} from the measurement of the Lamb shift $\Delta E(2S - 2P)$ using equation (1.1).

4.3 Alternate P_{NR} Expansion

We now present preliminary results obtained from the alternate P_{NR} expansion described in Section 3.4 . In Figure 4.6 the response functions $R_\ell(q)$ of equation (3.110) corresponding to $\ell = 0$ and $\ell = 1$ are plotted using the N^{3}LO-EM potential with $N_{\text{Max}} = 100$, $\hbar\Omega = 8$ MeV.

The $R_{\ell=1}(q)$ response function is observed to be larger than the $R_{\ell=0}(q)$, and dominated by values at $q = 0$ confirming the dominance of the dipole corrections over other multipole corrections. The results of integrating the response functions are given in Table 4.8.

[1] When the addition of the terms in δ_{TPE} is considered to fewer decimal places the sum is $\delta_{TPE} = -1.714 \pm 0.022$ meV

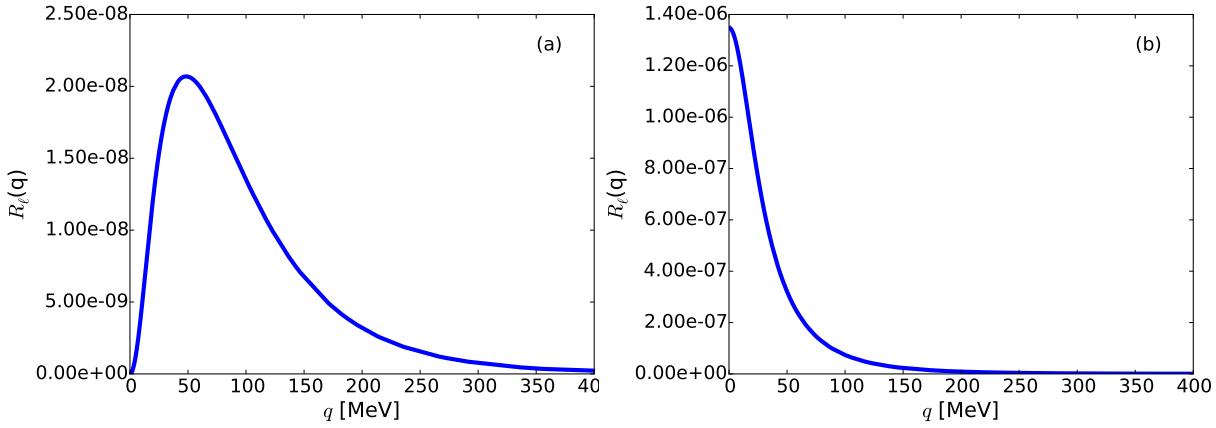

Figure 4.6: Plots of the deuteron response function $R_\ell(q)$ vs q for (a) $\ell = 0$ and (b) $\ell = 1$.

N^{3}LO-EM	$\delta^{(0)}_{\ell=0}$	$\delta^{(0)}_{\ell=1}$	$\delta^{(0)}_{\ell=2}$	$\delta^{(0)}_{\ell=3}$	$\delta^{(0)}_{\ell=4}$	$\sum \delta^{(0)}_{\ell}$
[meV]	-0.069	-1.436	-0.064	-0.012	-0.004	-1.585

Table 4.8: Nuclear polarizability contributions using alternate P_{NR} expansion.

In this formalism $\delta^{(1)}_{Z3}$ is implicitly included. Therefore, to compare these results with our previous method we add this term to our non-relativistic corrections $\delta_{NR} = \delta^{(0)}_{D1} + \delta^{(2)}_{R2} + \delta^{(2)}_{Q} + \delta^{(2)}_{D1D3} + \delta^{(1)}_{Z3} = -1.592$ meV. This result differs from $\sum_\ell \delta_\ell$ by 0.44%. These preliminary results suggest that this alternate method will be useful for calculating all higher order nuclear structure corrections at the cost of being more computationally expensive. It has been found numerically that the expansion in $|\boldsymbol{R} - \boldsymbol{R}'|$ for ^{3}H and ^{3}He display very different convergence [60] patterns therefore the formalism that was developed in Section 3.2 may potentially yield a convergence problem in larger A systems. This alternate approach provides an independent test of our calculations using the $|\boldsymbol{R} - \boldsymbol{R}'|$ expansions.

Chapter 5

Conclusions and Outlook

We have worked out in detail the formalism required to calculate the nuclear polarizability corrections in light muonic atoms and have applied it to the deuteron. The work of Leidemann and Rosenfelder [61] were among the earliest attempts to calculate these corrections and estimated the potential dependence to be less than 2%. However, their analysis missed important corrections, such as the Coulomb and finite nucleon size corrections and since then the modern approach of χ_{EFT} has provided a new way to derive NN potentials rooted in QCD. We have been able to provide all of the relevant nuclear structure corrections $\delta^A_{pol}+\delta_{Zem}$ for μD using the new generation, state-of-the-art nuclear potentials derived from chiral perturbation theory and the AV18 potential [57]. This work has allowed us to place robust constraints on our final result $\delta_{TPE} = -1.716 \pm 0.022(1\sigma)$ meV. We have performed rigorous benchmarks on our numerics by comparing our work to that of Refs. [36, 40, 52] for ground state properties, and to Refs. [26, 55, 56] for the excited state properties. These numerical tests have allowed us to check our results and those of Pachucki.

After his last paper [58] and discussions with other experts we have agreed on the best value of the elastic and inelastic proton and neutron contributions to add. This is key for the experimental program at PSI.

Having finalised our study of nuclear polarizability corrections to the Lamb shift of muonic deuterium, in future work we would like to address the nuclear structure corrections pertinent to other atomic transitions, such as the hyperfine splitting (HF) in light muonic atoms. The HF splitting is the energy difference between two different states of lepton-nucleus total angular momentum (F, M_F) in an atom and has been measured experimentally for muonic hydrogen and deuterium [6, 7]. Unlike the Lamb shift, the HF splitting is dominated by magnetic transitions which are sensitive to meson-exchange currents. Consequently, to achieve the precision required by experiments, meson exchange currents must be incorporated into the calculation. The theoretical description of the HF splitting in electronic atoms has been accomplished by Pachucki [62] and Friar [63], however, it has not yet been applied to the muonic case. Some simpler calculation of nuclear structure are included in Ref. [64]. We plan to extend the formalism to the case of few-body muonic atoms, taking into account the meson exchange currents, and obtain the nuclear structure corrections using state-of-the-art nuclear forces derived from χ_{EFT}. The HF splitting will be measured also on ^{3}He in the future so this would open up the possibility of further collaboration with the experimentalists.

Appendix A

Angular Momentum Theory

In this appendix we give a brief overview of spherical tensors, spherical harmonic vectors, the Wigner-Eckart theorem and provide some of the reduced matrix elements of operators that were used to collect the results of the main text.

An irreducible spherical tensor operator of rank k, $(k \in \mathcal{N})$, is defined as the set of operators $\{T_q^{(k)}; q = -k, \ldots k\}$ that satisfy the following commutation relations:

$$\left[\hat{J}_z, T_q^{(k)}\right] = qT_q^{(k)}, \tag{A.1}$$

$$\left[\hat{J}_\pm, T_q^{(k)}\right] = \sqrt{k(k+1) - q(q \pm 1)}T_{q\pm1}^{(k)}. \tag{A.2}$$

Two irreducible spherical tensors of rank k_1 and k_2 can be combined to yield another irreducible spherical tensor of rank $p = \{|k_1 - k_2|, \ldots, k_1 + k_2\}$ through,

$$T_\mu^p = \left[A^{(k_1)} \times B^{(k_2)}\right]_\mu^p = \sum_{q_1,q_2} \langle k_1, m_1, k_2, m_2 | p, \mu \rangle A_{q_1}^{(k_1)} B_{q_2}^{(k_2)}, \tag{A.3}$$

where $\langle k_1, m_1, k_2, m_2 | p, \mu \rangle$ is the Clebsch-Gordan coefficient.

A.1 The Wigner-Eckart Theorem

In the following, we give a list of several useful results from Ref. [65],

$$\sum_{M,\nu} |\langle k\nu JM|J_0M_0\rangle|^2 = 1 \ , \tag{A.4}$$

$$\langle k-\nu JM|J_0M_0\rangle = \sqrt{\frac{2J_0+1}{2J+1}}(-1)^{\nu+J_0-J}\langle k\nu JM|J_0M_0\rangle \ . \tag{A.5}$$

The Wigner-Eckart theorem is given as Ref. [65], by

$$\langle N_0J_0M_0|T^{(k)}_\nu|NJM\rangle = (-1)^{k-J+J_0}\frac{\langle k\nu JM|J_0M_0\rangle}{\sqrt{2J_0+1}}\langle N_0J_0||T^{(k)}||NJ\rangle \ , \tag{A.6}$$

where $\langle N_0J_0||T^{(k)}||NJ\rangle$ is the reduced matrix element. A useful identity is

$$\sum_m \langle N_0J_0|A^{(k)}_m|NJ\rangle\langle N_0J_0|B^{(k)}_m|NJ\rangle = \frac{(-1)^{J_0-J}}{2J_0+1}\langle N_0J_0||A^{(k)}||NJ\rangle\langle N_0J_0||B^{(k)}||NJ\rangle. \tag{A.7}$$

A.2 Spherical Harmonics

The spherical harmonics, $Y^\ell_m(\hat{r})$ are irreducible rank (ℓ) spherical tensor operators that satisfy the following properties:

$$Y^{\ell*}_m(\hat{r}) = (-1)^m Y^\ell_{-m}(\hat{r}), \tag{A.8}$$

$$\int d\hat{r}\ Y^\ell_m(\hat{r})Y^{\ell'}_{m'}(\hat{r}) = \delta_{m,m'}\delta_{\ell,\ell'}. \tag{A.9}$$

The spherical harmonics can be written in terms of associated Legendre polynomials, $P^\ell_m(x)$, as:

$$Y^\ell_m(\hat{r}) = (-1)^m\sqrt{\frac{(2\ell+1)}{4\pi}\frac{(\ell-m)!}{(\ell+m)!}}P^\ell_m(\cos(\theta))e^{im\phi}. \tag{A.10}$$

A.3 Vector Spherical Harmonics

A vector spherical harmonic $\boldsymbol{Y}^M_{J\ell}(\hat{x})$ is defined as the tensor product of a spherical harmonic of rank (ℓ) with the rank (1) spherical vector basis $\hat{e}_\lambda$,

$$\boldsymbol{Y}^M_{J\ell}(\hat{x}) = \left[Y^\ell_m \times \hat{e}_\lambda\right]^J_M = \sum_{m,\lambda} \langle \ell m, 1\lambda | JM \rangle Y^\ell_m(\hat{x}) \hat{e}_\lambda. \tag{A.11}$$

where we have

$$\hat{e}_{\pm 1} = \mp \frac{1}{\sqrt{2}}(\hat{x} \pm i\hat{y}), \tag{A.12}$$

$$\hat{e}_0 = \hat{z}. \tag{A.13}$$

The spherical vector harmonics satisfy the following orthogonality properties,

$$\int d\Omega \; \boldsymbol{Y}^{M'*}_{J'\ell'}(\hat{x}) \cdot \boldsymbol{Y}^M_{J\ell}(\hat{x}) = \delta^J_{J'} \delta^{M'}_M \delta^{\ell'}_\ell, \tag{A.14}$$

$$\sum_{J\ell M} \boldsymbol{Y}^{M*}_{J,\ell}(\hat{x}) \boldsymbol{Y}^M_{J,\ell}(\hat{x}') = \hat{I} \delta(\Omega_{\hat{x}} - \Omega_{\hat{x}'}). \tag{A.15}$$

In addition, $\boldsymbol{Y}^{M'*}_{J'\ell'}(\hat{x})$ also satisfies,

$$\hat{J}_z \boldsymbol{Y}^M_{J\ell}(\hat{r}) = M \boldsymbol{Y}^M_{J\ell}(\hat{r}) \tag{A.16}$$

$$\hat{J}^2 \boldsymbol{Y}^M_{J\ell}(\hat{r}) = J(J+1) \boldsymbol{Y}^M_{J\ell}(\hat{r}) \tag{A.17}$$

$$\hat{L}^2 \boldsymbol{Y}^M_{J\ell}(\hat{r}) = \ell(\ell+1) \boldsymbol{Y}^M_{J\ell}(\hat{r}) \tag{A.18}$$

$$\boldsymbol{S}^2 \boldsymbol{Y}^M_{J\ell}(\hat{r}) = 2 \boldsymbol{Y}^M_{J\ell}(\hat{r}) \tag{A.19}$$

$$\tag{A.20}$$

Bibliography

[1] I. Sick, *Physics Letters B*, vol. 576, no. 12, pp. 62-67, 2003.

[2] R. Rosenfelder, *Physics Letters B*, vol. 479, no. 4, pp. 381-386, 2000.

[3] I. Sick, *Progress in Particle and Nuclear Physics*, vol. 67, no. 2, pp. 473-478, 2012.

[4] J. C. Bernauer, *Doctoral Dissertation*, 2010.

[5] P. Mohr *et al.*, *Rev. Mod. Phys.*, vol. 84, no. 1527, 2012.

[6] R. Pohl *et al.*, *Nature*, vol. 466, pp. 213-216, 2010.

[7] A. Antognini *et al.*, *Science*, vol. 339, p. 417, 2013.

[8] J. C. Bernauer *et al.*, *Phys. Rev. Lett.*, vol. 105, p. 242001, 2010.

[9] X. Zhan *et al.*, *Physics Letters B*, vol. 705, no. 12, pp. 59-64, 2011.

[10] I. Lorenz, H.-W. Hammer, and U.- G. Meißner , *Eur. Phy. J. A*, vol. 48, p. 151, 2011.

[11] E. Kraus, K. E. Mesick, A. White, R. Gilman, and S. Strauch, *Phys. Rev. C*, vol. 90, p. 045206, Oct 2014.

[12] J. P. Miller, E. de Rafael, B. L. Roberts, and D. Stöckinger, Annu. Rev. Nucl. Part. Sci., vol. 62, pp. 237-264, 2012.

[13] B. Batell, D. Mckeen, and M. Pospelov, *P.R.L.*, vol. 107, no. 011803, 2011.

[14] D. Tucker-Smith and I. Yavin, *Phys. Rev. D*, vol. 83, no. 101702, 2011.

[15] A. Antognini *et al.*, Can. J. Phys., vol. 89, p. 47, 2011.

[16] R. Pohl, R. Gilman, G. Miller, and K. Pachucki, *Annu. Rev. Nucl. Part. Sci.*, vol. 63, 2013.

[17] J. J. Krauth, M. Diepold, B. Franke, A. Antognini, F. Kottmann, and R. Pohl, *arXiv:1506.01298*, 2015.

[18] C. E. Carlson *Phys. Rev. A*, vol. 89, no. 022504, 2014.

[19] J. Friar, J. Martorell, and D. W. L. Sprung, *Phys. Rev. A*, vol. 56, pp. 4579-4586, 1997.

[20] K. Pachucki *Phys. Rev. Lett.*, vol. 106, no. 193007, 2011.

[21] G. Audi, O. Bersillon, J. Blachot, and A. Wapstra, *Nuclear Physics A*, vol. 624, no. 1, 1997.

[22] M. Pavanello, W.-C. Tung, and L. Adamowicz, *Phys. Rev. A*, vol. 81, no. 042526, 2010.

[23] M. Garçon and J. V. Orden, *nucl-th:0102049*, 2001.

[24] U. Jentschura, C. P. A. Matveev, J. Alnis, R. Pohl, T. Udem, N. Kolachevsky, and T. Hänsch, *Phys. Rev. A*, vol. 83, no. 042505, 2011.

[25] G.E. Brown and A.D. Jackson, *The Nucleon-Nucleon Interaction*. Amsterdam: North-Holland Pub., 1976.

[26] H. Arenhövel and M. Sanzone, *The photodisintegration of the deuteron*, *Few Body Systems*, vol. 3, p. 1, 1991.

[27] H. A. Bethe, *Phys. Rev.*, vol. 76, p. 38, 1949.

[28] I. Khriplovich, *Physics of Atomic Nuclei*, vol. 64, no. 3, pp. 516-524, 2001.

[29] I. Khriplovich, *Theoretical Kaleidoscope*. New York: Springer Science Business Media, 2008.

[30] J. Friar, *Phys. Rev. C*, vol. 88, p. 034003, 2013.

[31] N. Zettili, *Quantum Mechanics*. UK: John Wiley and Sons Ltd, 2009.

[32] S. Wong, *Introductory Nuclear Physics*. Prentice Hall, 1990.

[33] H. Yukawa, *Proc. Phys. Math. Soc.*, vol. 17, p. 48, 1935.

[34] R. Machleidt, *The meson theory of nuclear forces and nuclear structure*, in Advances in Nuclear Physics (J.W Negele and E. Vogt, ed.), vol. 19, Springer US, 1989.

[35] S. Okubo and R. Marshak, *Ann. Phys.*, vol. 4, pp. 166-179, 1958.

[36] R. Wiringa, V. Stoks, and R. Schiavilla *Phys. Rev. C*, vol. 51, no. 1, 1995.

[37] S. Weinberg, *Phys. Lett. B*, vol. 251, p. 288, 1990.

[38] S. Weinberg, *Nuclear Phys. Lett. B*, vol. 363, p. 3, 1991.

[39] R. Machleidt and D. Entem, *Phys. Rep.*, vol. 503, pp. 1-75, 2011.

[40] D. Entem and R. Machleidt, *Phys. Rev. C*, vol. 68, no. 041001, 2003.

[41] F. Gross, *Relativistic Quantum Mechanics and Field Theory*. New York: Wiley, 1999.

[42] M. I. Eides, H. Grotch, and V. A. Shelyuto, *Phys. Rep.*, vol. 342, pp. 63-261, 2001.

[43] E. Borie, *Ann. Phys.*, vol. 327, pp. 733-763, 2012.

[44] R. Karplus, A. Klein, and J. Schwinger, *Phys. Rev.*, vol. 86, 1952.

[45] J. Friar, *Annals of Physics*, vol. 122, pp. 151-196, 1979.

[46] R. Hill, *Hydrogenic wave functions*, in *Springer Handbook of Atomic, Molecular, and Optical Physics* (G. Drake, ed.), Springer, 2005.

[47] C. Ji, N. N. Dinur, S. Bacca, and N. Barnea, *Manuscript in preparation.*

[48] R. Rosenfelder, *Nucl. Phys. A.*, vol. 393, pp. 301-313, 1983.

[49] R. Rosenfelder, *Muonic polarization in muonic atoms*, in *Muonic Atoms and Molecules* (L. Schaller and C. Petitjean, eds.), Birkhauser Basel, 1993.

[50] J. D. Walecka, *Theoretical and Subnuclear Physics*. London: Imperial College, 2004.

[51] S. Galster, H. Klein, J. Moritz, K. Schmidt, D. Wegener, and J. Bleckwenn, *Nuc. Phys. B.*, vol. 32, no. 1, 1971.

[52] E. Epelbaum, W. Glockle, and U.-G. Meibner,*Nuclear Physics A*, vol. 747, p. 362, 2005.

[53] *Private Communications with Epelbaum.*

[54] H. Arenhövel, *Electromagnetic interactions of nucleons and nuclei at low energy and momentum transfer*, in *Substructures of Matter as Revealed with Electroweak Probes* (L. Mathelitsch and W. Plessas, eds.), Lecture Notes in Physics, 2005.

[55] J. L. Friar and G. Payne, *Phys. Rev. C*, vol. 55, no. 2764, 1997.

[56] J. L. Friar and G. Payne, *Phys. Rev. C*, vol. 56, no. 2, p. 619, 1997.

[57] O. J. Hernandez, C. Ji, S. Bacca, N. N. Dinur, and N. Barnea, *Phys. Lett. B.*, vol. 736, pp. 344-349, 2014.

[58] K. Pachucki and A. Wienczek, *Phys. Rev. A.*, vol. 91, no. 040503, 2015.

[59] *Private Communications with Arenhövel.*

[60] N. N. Dinur, C. Ji, S. Bacca, and N. Barnea, *Manuscript in preparation.*

[61] W. Leidemann and R. Rosenfelder, *Phys. Rev. C*, vol. 427, 1995.

[62] K. Pachucki, *Phys. Rev. A*, vol. 76, no. 022508, 2007.

[63] J. L. Friar and G. L. Payne, *Phys. Rev. C*, vol. 72, no. 014002, 2005.

[64] R. Faustov, A. Martynenko, G. Martynenko, and V. Sorokin, *Phys. Rev. A*, vol. 90, no. 012520, 2014.

[65] A. R. Edmonds, *Angular Momentum in Quantum Mechanics*. Princeton: Princeton University Press, 1996.